Synaptonemal complex architecture facilitates the chromosome-specific regulation of recombination in Drosophila

Cori K. Cahoon*, G. Matthew Heenan*, Zulin Yu*, Jay R. Unruh*, Sean McKinney*, and R. Scott Hawley*,‡

* Stowers Institute for Medical Research, Kansas City, MO, United States of America

‡ Department of Molecular and Integrative Physiology, University of Kansas Medical Center, Kansas City, KS, United States of America

Corresponding Author:

R. Scott Hawley

Stowers Institute for Medical Research

Kansas City, MO 64110

Phone (816) 926-4427

Fax (816) 926-2060

rsh@stowers.org

Key words: synaptonemal complex, meiosis, homologous recombination, crossover, crossover interference

Abstract

In Drosophila, meiotic recombination is initiated by the formation of programmed DNA double-strand breaks (DSBs), which occur within the context of the synaptonemal complex (SC). To better understand the role of the SC in mediating recombination we created an in-frame deletion mutant in *c(3)G* (deleting amino acids L340 to N550, denoted as *c(3)G*$^{cc\Delta 1}$), which encodes the major transverse filament protein of the SC. Although *c(3)G*$^{cc\Delta 1}$ oocytes assemble ribbon-like SC and exhibit normal DSB formation, the euchromatic SC precociously disassembles into fragments that persist until mid to late pachytene in both *c(3)G*$^{cc\Delta 1}$ heterozygotes and homozygotes. Centromeric SC, however, is unaffected in both genotypes. Thus, *c(3)G*$^{cc\Delta 1}$ is a separation-of-function mutant that establishes different functional and structural requirements between euchromatic and centromeric SC. Our data also demonstrate that the chromosome arms differ in their sensitivity to *c(3)G*$^{cc\Delta 1}$-induced perturbations in the SC. The *X* chromosome is distinctly sensitive to these perturbations, such that euchromatic pairing and crossing over are altered in *c(3)G*$^{cc\Delta 1}$ heterozygotes and severely reduced in *c(3)G*$^{cc\Delta 1}$ homozygotes. On the autosomes, crossovers are shifted to centromere-proximal regions and crossover interference is defective in both *c(3)G*$^{cc\Delta 1}$ homozygotes and heterozygotes. However, only *c(3)G*$^{cc\Delta 1}$ homozygotes display a progressive loss of euchromatic pairing in distal autosomal regions, suggesting that discontinuity in the euchromatic SC—rather than failed pairing—might cause the altered crossover distribution. These phenotypes reveal that different chromatin states or regions have differing requirements to maintain both the SC and homologous pairing. Furthermore, *c(3)G*$^{cc\Delta 1}$ is the first mutant in Drosophila to demonstrate that the SC appears to facilitate the regulation of recombination frequency and distribution differently on each chromosome.

Author Summary

Chromosome segregation errors during meiosis are the leading cause of miscarriage and birth defects in humans. To prevent these errors from occurring, meiotic cells have evolved multiple mechanisms to ensure that each gamete receives exactly half the number of chromosomes. During meiosis I, this is accomplished by forming a crossover between homologous chromosomes, which is facilitated by a large protein complex called the synaptonemal complex (SC). The SC is assembled between homologous chromosomes during early prophase I, and it is unclear how the SC regulates the position and number of crossovers each homolog receives. To better understand the role of the SC in mediating recombination, we created an in-frame deletion mutant in *Drosophila melanogaster* in the gene encoding the C(3)G protein, the major transverse filament protein of the SC. Although mutant oocytes assemble ribbon-like SC, the SC along the chromosome arms precociously disassembles in early meiosis. Surprisingly, the SC around the centromeres is unaffected in these mutants, suggesting that the requirements for SC formation may differ depending on where the SC is located along the chromosomes. Our data also demonstrate that the chromosome arms differ in their sensitivity to the mutant-induced perturbations of the SC in both crossing over and homolog pairing.

INTRODUCTION

At the beginning of meiotic prophase, homologous chromosomes must identify each other, pair, and initiate recombination. Meiotic recombination is critical for the proper segregation of homologous chromosomes during meiosis I. The failure to properly exchange genetic information will frequently result in missegregation of the chromosomes leading to eggs and sperm with the incorrect number of chromosomes. Indeed, errors in meiotic chromosome segregation are the leading cause of miscarriage and aneuploidy in humans, which can result in chromosomal disorders such as Down syndrome and Turner syndrome (reviewed in [1]).

To initiate recombination, a series of programmed DNA double-strand breaks (DSBs) are formed by the topoisomerase-like enzyme Spo11 [2]. Most organisms make a large excess of DSBs—in some cases 30 times more than necessary—since only a small fraction of DSBs will be repaired into crossovers [reviewed in 3]. Some organisms appear to use DSBs to identify homology, and it is thought that creating more DSBs than necessary helps to ensure that homologs are able to properly pair and that each chromosome receives at least one crossover [reviewed in 4].

Neither DSBs nor crossovers are randomly distributed along chromosome arms, but rather seem to be placed in a fairly ordered manner. Fine-scale genomic analysis of the nonrandom distribution of DSBs in mice and yeast has indicated that the location of DSBs involves a complicated series of factors working together on both a local DNA sequence level and on a global chromatin architecture level [5, 6]. Moreover, the nonrandom distribution of the resulting crossovers varies depending on the organism. Some organisms, like Drosophila, place most of their crossovers in the middle of the chromosome arms, while other organisms, like grasshoppers, planarians and nematodes, position crossovers at the distal regions of chromosome arms [reviewed in 7] [8]. This suggests that there may be multiple mechanisms

86 that can determine the position of DSBs along the chromosome arms and that only certain
87 DSBs can become crossovers.

88 In Drosophila, approximately one crossover forms per chromosome arm [9, 10]. The
89 tight regulation of crossover number is controlled by multiple processes, including crossover
90 interference, the centromere effect, and region-specific constraints [reviewed in 11]. Once a
91 crossover has formed, crossover interference functions to suppress the formation of additional
92 crossovers nearby. Similarly, the centromere effect and regional constraints function to prevent
93 the formation of crossovers in or next to specific chromatin states, such as the centromere and
94 heterochromatin. All of these processes function over megabases of DNA to constrain the
95 crossover number in each meiosis to an average of six crossovers across the three crossover-
96 competent chromosomes in Drosophila. Exactly how interference, the centromere effect, and
97 region-specific constraints function is not well understood.

98 Double-strand break formation and crossing over in Drosophila occur within the context
99 of full-length synaptonemal complex (SC) (Fig 1A) [15, 16]. The SC, a large protein complex
100 that assembles between paired homologous chromosomes, is required for the formation of
101 crossovers. It is therefore possible that the SC may play a role in regulating the crossover fate
102 of DSBs. Additionally, the SC connects two homologs along their entire lengths, making it an
103 ideal candidate structure for monitoring DSB formation and crossover maturation occurring at
104 different places along the chromosomes. Indeed, several studies have strongly suggested the
105 SC plays a role in mediating crossover interference [17, 18].

106 The synaptonemal complex is arranged in three parts: lateral elements (LEs), a central
107 region (CR), and a central element (CE) (Fig 1B). The LEs assemble on each homolog
108 alongside the axis components, which consist of cohesin and cohesin-like proteins that are
109 thought to establish the meiotic chromatin architecture [reviewed in 19, 20]. The LEs interact

110 with the CR proteins, which occupy the space between the two homologs. Transverse filament
111 proteins span the distance of the CR, thereby connecting the LEs of each homolog. In the
112 middle of the CR is the CE, which consists of proteins that are thought to help stabilize the
113 transverse filaments.

114 Genetic analyses have identified multiple components of the Drosophila SC, and recent
115 advances in superresolution microscopy have allowed SC components to be precisely
116 positioned within the overall SC structure (Fig 1B). The Drosophila SC forms two layers that are
117 mirror images of one another [21]. C(3)G, the major transverse filament protein of the
118 Drosophila SC [22], forms a homodimer, with the C-terminal ends of each subunit positioned in
119 the LE and the N-terminal ends in the CE [23]. The N terminus of one homodimer is then
120 thought to interact with the N terminus of another homodimer to span the distance between the
121 two homologs, thus connecting the two homologous LEs [23]. It is currently unclear exactly how
122 C(3)G interacts with the LE. An additional CR protein, Corolla, was recently identified [24].
123 Corolla, resides within the CR as two parallel tracks and has been shown by yeast two-hybrid
124 analysis to interact with the CE protein Corona (CONA) [21, 24, 25], which also forms two
125 parallel tracks within the CE [21, 26]. C(3)G, Corolla, and CONA depend on each other in order
126 to assemble the SC, and all three proteins are required for the formation of crossovers [22, 24-
127 26].

128 The first step toward dissecting the functional anatomy of the C(3)G protein involved
129 creating in-frame deletion mutations, which showed that the N- and C-terminal globular domains
130 of C(3)G are required to properly assemble the SC and for robust crossover formation [27].
131 Here, we describe the effects of a mutant, $c(3)G^{cc\Delta 1}$, with an in-frame deletion of a coiled-coil
132 domain. To properly characterize this mutant, we created a CRISPR/Cas9 allele, eliminating
133 any of the common concerns regarding levels of expression that are inherent when using a

134 randomly inserted transgene. (A transgene in-frame deletion mutant, similar to the one in this
135 manuscript, has been previously created, but was never extensively analyzed [22]).

136 *c(3)G*$^{cc\Delta 1}$ removes 211 amino acids from the largest coil-coiled domain of C(3)G which,
137 as a homozygote, shortens the width of the SC by ~40 nm and thus reduces the distance
138 between the homologs. Both heterozygotes and homozygotes of *c(3)G*$^{cc\Delta 1}$ are able to assemble
139 the SC, display normal DSB formation, and affect neither the persistence of SC at the
140 centromere nor centromere clustering. However, euchromatic SC disassembles prematurely in
141 both genotypes, resulting in fragmented or discontinuous SC along the length of the
142 chromosomes. This premature SC disassembly affects both homolog pairing and recombination,
143 but to different degrees on each chromosome. *c(3)G*$^{cc\Delta 1}$ is the first Drosophila mutant to
144 illustrate a chromosome-specific regulation of recombination, where each chromosome has
145 different requirements for the SC in maintaining homolog pairing and facilitating recombination.

146

147 **RESULTS**

148 **Novel loss-of-function allele of *c(3)G* affects the width of the SC**

149 A large deletion in the yeast transverse filament protein Zip1 decreases the distance between
150 the LEs, suggesting that Zip1 is directly involved in determining the width of the SC [28]. Since
151 Zip1 and C(3)G are functional homologs of each other, we postulated that a similar deletion in
152 C(3)G may alter the Drosophila SC in a similar manner to the Zip1 deletion in yeast. To that
153 end, we created a CRISPR/Cas9-mediated in-frame deletion in the Drosophila *c(3)G* gene (see
154 Methods) that removes 211 amino acids from the second coiled-coil domain in C(3)G (Fig 1B).
155 We call this mutant *c(3)G*$^{cc\Delta 1}$.

156 Based on the 1.485-angstrom size of an amino acid in a coiled-coil, the mathematically
157 calculated decrease in SC width expected by deleting 211 amino acids from a coiled-coil
158 configuration is ~63 nm. However, when using single-molecule superresolution techniques such
159 as stochastic optical reconstruction microscopy (STORM), which require primary and secondary
160 antibodies, the size of an antibody complex (20–30 nm) will introduce uncertainty into the
161 precise positioning of the structure being imaged. To account for this, we added the size of the
162 primary and secondary antibody complex, which recognizes the C-terminus C(3)G, to the
163 calculated decrease in SC width resulting in an expected decrease of ~43–53 nm in *c(3)G*$^{cc\Delta 1}$
164 homozygotes.

165 Using STORM on intact germaria with an antibody that recognizes the C-terminal end of
166 C(3)G, we observed two tracks of the C(3)G C-termini, suggesting that the SC was able to
167 assemble both C(3)G homodimers (Fig 2). Additionally, when we measured the distance
168 between these two tracks, referred to as the SC width, it was decreased by ~40 nm in *c(3)G*$^{cc\Delta 1}$
169 homozygotes (Fig 2; wild type, 119 nm ± SE 1.0; *c(3)G*$^{cc\Delta 1}$, 78.6 nm ± SE 0.3; P<0.0001), which
170 closely matched the expected decrease in SC width. This suggests that, like Zip1, C(3)G is
171 responsible for determining the distance between the LEs in Drosophila.

172 STORM analysis of *c(3)G*$^{cc\Delta 1}$ heterozygotes, in which flies express one *c(3)G*$^{cc\Delta 1}$ version
173 and one wild type (WT) version of C(3)G, showed an intermediate change in SC width (Fig 2;
174 107 nm ± SE 0.4; P<0.0001 when compared to WT). This suggests that *c(3)G*$^{cc\Delta 1}$ heterozygotes
175 incorporate a combination of *c(3)G*$^{cc\Delta 1}$ and WT versions of C(3)G into the SC. One possible way
176 to accomplish this heterogeneity would be to alternate the C(3)G tetramers such that every
177 other tetramer is the *c(3)G*$^{cc\Delta 1}$ mutant. In this case, we would expect the profiles on either C-
178 terminal side of C(3)G to be thicker. However, this is not likely to be the case because the
179 thicknesses of the C-terminal C(3)G signal are nearly the same for the *c(3)G*$^{cc\Delta 1}$ heterozygotes
180 and homozygotes (WT: 62 nm; *c(3)G*$^{cc\Delta 1}$ heterozygote: 49 nm; *c(3)G*$^{cc\Delta 1}$ homozygotes: 43 nm).

181 It is also possible that *c(3)G*$^{cc\Delta 1}$ and WT C(3)G monomers are able to dimerize and create mixed
182 C(3)G homodimers, or that the N termini of *c(3)G*$^{cc\Delta 1}$ homodimers can interact with the N termini
183 of WT homodimers in the CE of the SC to create a mixed tetramer. Both possibilities would
184 result in the intermediate SC width seen in *c(3)G*$^{cc\Delta 1}$ heterozygotes. Given the heterogeneous
185 nature of STORM data, it is impossible to distinguish between these possibilities. Further
186 studies with alternative methodologies will be needed to gain a more detailed understanding of
187 this ultrastructure.

188 Both *c(3)G*$^{cc\Delta 1}$ heterozygotes and homozygotes initiate SC assembly at the centromeres
189 during the pre-meiotic mitotic divisions (region 1) and at the onset of meiosis in zygotene/early
190 pachytene (region 2A) assembled ribbon-like SC with normal kinetics (Fig 3). Moreover, further
191 analysis of the SC in region 2A by measuring the intensity of the antibody staining of Corolla
192 between the mutants and WT showed that although the SC appeared to be ribbon-like in the
193 mutants the intensity was decreased compared to WT (Fig S1). This suggested either that both
194 *c(3)G*$^{cc\Delta 1}$ heterozygotes and homozygotes may not be assembling as much SC as in WT or that
195 both mutants have altered the tripartite structure of the SC. However, based on our ability to
196 resolve two C(3)G C-terminal tracks in the STORM data and on Corolla being able to assemble
197 into ribbon-like SC in the deconvolution microscopy data (Fig 3, Figure S1), we do not believe
198 that the decrease in SC intensity indicates a lack of tripartite SC. All of the known components
199 of the SC in Drosophila are co-dependent on each other to be able to assemble, thus if the
200 structure of the SC was failing in these mutants then we would expect both C(3)G and Corolla to
201 be unable to assemble into ribbon-like SC [24, 25].

202

203 ***c(3)G*$^{cc\Delta 1}$ affects the persistence of SC along the chromosome arms but not at the**
204 **centromere**

205 Previous studies have shown that *c(3)G* null mutants initiate DSBs, but at reduced levels
206 compared to WT [16, 29]. This suggests that some DSBs will only form in the presence of SC.
207 In *c(3)G*$^{cc\Delta 1}$ heterozygotes and homozygotes, DSB formation appears to be normal. To identify
208 DSBs, we used an antibody that recognizes the phosphorylated form of the histone variant
209 H2AV (referred to as γH2AV), and this phosphorylation mark is one of the first events that
210 occurs following the formation of DSBs [30]. At zygotene/early pachytene (region 2A) all 16-cells
211 within the cyst will induce DSBs, and for this assay we scored only DSBs in the meiotic cells,
212 were identified by the presence of the SC [16]. Nurse cells also induce DSBs, but they do not
213 assemble the SC and were excluded from this analysis [16].

214 In an otherwise WT background, both *c(3)G*$^{cc\Delta 1}$ heterozygotes and homozygotes
215 displayed near WT levels of γH2AV foci in zygotene/early pachytene (region 2A) (Fig S2; WT=
216 average 6 ± SE 0.6; *c(3)G*$^{cc\Delta 1}$ homozygotes= average 6 ± SE 0.6, P=0.77; *c(3)G*$^{cc\Delta 1}$
217 heterozygotes= average 7 ± SE 0.8, P=0.69). By early pachytene (region 2B), the number of
218 γH2AV foci was reduced to ~1 focus in WT (average 1 ± SE 0.3) and *c(3)G*$^{cc\Delta 1}$ heterozygotes
219 (average 1 ± SE 0.2, P=0.06). *c(3)G*$^{cc\Delta 1}$ homozygotes displayed a wider range of γH2AV foci
220 with an average of 3 DSBs (± SE 0.5) in early pachytene (region 2B). This was statistically
221 different from WT (P=0.036), but it is unclear if this indicates a delay in DSB repair or the
222 initiation of more DSBs. By mid pachytene (region 3) all γH2AV foci were absent in both
223 *c(3)G*$^{cc\Delta 1}$ homozygotes (P=0.54) and heterozygotes (P=0.17). Thus, while *c(3)G*$^{cc\Delta 1}$
224 homozygotes may have some anomalies in DSB repair or late-DSB initiation in early pachytene,
225 by mid pachytene the repair of these breaks follows similar to WT timing.

226 In WT, euchromatic SC initiates disassembly in mid/late pachytene (stages 5–7) and the
227 SC is fully disassembled from the chromosome arms by stages 8–9. Interestingly, both *c(3)G*$^{cc\Delta 1}$
228 homozygotes and heterozygotes initiated premature disassembly of euchromatic SC as cells
229 progressed into early and mid pachytene (Fig 3). *c(3)G*$^{cc\Delta 1}$ homozygotes began to initiate

230 euchromatic SC disassembly in early pachytene (region 2B), whereas *c(3)G*$^{cc\Delta 1}$ heterozygotes
231 started disassembling euchromatic SC in mid pachytene (region 3). Furthermore, this pattern
232 was recapitulated when the antibody intensity of Corolla was quantified in each mutant at each
233 stage of meiosis (Fig S1). Thus, the presence of one WT copy of C(3)G in a *c(3)G*$^{cc\Delta 1}$
234 heterozygote delays the onset of premature SC disassembly but cannot fully rescue the defect,
235 demonstrating the semi-dominant nature of the *c(3)G*$^{cc\Delta 1}$ mutant. In both homozygotes and
236 heterozygotes, the fragmented SC persisted until stages 5–7 (mid/late pachytene) and was fully
237 disassembled by stages 8–9, similar to when euchromatic SC is normally disassembled from
238 the chromosome arms (Fig 3; Fig S1). Surprisingly, *c(3)G*$^{cc\Delta 1}$ mutants were able to maintain SC
239 at the centromeres, suggesting that the SC at the centromere is unaffected by this deletion.

240 In Drosophila, centromeres begin to homologously pair and initiate the assembly of
241 centromeric SC during the four premeiotic mitotic divisions (region 1) (Fig 1A, Fig 3)[13]. At the
242 transition from the premeiotic divisions to meiotic prophase (region 2A) the paired centromeres
243 cluster together into 1–3 masses, and this process is dependent on SC assembly [12, 14]. Since
244 *c(3)G*$^{cc\Delta 1}$ homozygotes and heterozygotes were able to maintain the SC at the centromeres with
245 WT kinetics, we assayed centromere clustering to determine if this SC was functional. To do
246 this, we counted the number of centromere foci in nuclei containing SC using the centromeric
247 nucleosome Centromere identifier (CID) as a marker for the centromeres. In all of the stages
248 analyzed, centromere clustering was unaffected by the presence of *c(3)G*$^{cc\Delta 1}$ (Fig S3, Table
249 S1). Also, *c(3)G*$^{cc\Delta 1}$ did not display a dominant effect on centromere clustering when assayed as
250 a heterozygote (Fig S3, Table S1). For *c(3)G*$^{cc\Delta 1}$ homozygotes, we do observe an increase in
251 the number of nuclei with 3 centromeric foci in early pachytene. However, in the *c(3)G*^{68} null
252 mutant, most of the nuclei have 4 or more CID foci at this stage, which does not occur in the
253 *c(3)G*$^{cc\Delta 1}$ mutants [14]. Thus, these data demonstrate that centromeric SC is not dependent on
254 the deleted amino acids in *c(3)G*$^{cc\Delta 1}$ to function in clustering centromeres.

255 ***c(3)G^{ccΔ1}* causes defects in both recombination and euchromatic pairing on the *X***
256 **chromosome**

257 Previous studies have shown that in most (but not all) organisms the SC is required for the
258 formation of crossovers [reviewed in 19, 31]. In Drosophila, Gowen showed that flies
259 heterozygous for the *c(3)G* null mutation are indistinguishable from WT with respect to
260 recombination on all three crossover-competent chromosomes, demonstrating that one copy of
261 C(3)G is sufficient for normal recombination [32]. Moreover, flies homozygous for the *c(3)G* null
262 mutation are completely unable to repair DSBs into either crossovers or noncrossover gene
263 conversions on all three crossover competent chromosomes [16, 22, 32-34]. Therefore, the
264 question of how these breaks are repaired remains open [34].

265 Unlike *c(3)G* null mutants, *c(3)G^{ccΔ1}* does initially assemble ribbon-like SC, which
266 prematurely disassembles into fragments as the cells progress through early to mid pachytene.
267 To determine if the SC assembled in *c(3)G^{ccΔ1}*-bearing oocytes is able to promote crossing over,
268 we assayed for the presence of crossovers in both *c(3)G^{ccΔ1}* homozygotes and heterozygotes.
269 Interestingly, *c(3)G^{ccΔ1}* homozygotes and heterozygotes displayed different phenotypes with
270 regard to recombination on the *X* chromosome (Fig 4A; Table 1). Both genotypes were able to
271 from at least some crossovers, suggesting that the region deleted in *c(3)G^{ccΔ1}* is not required to
272 promote crossover formation per se. However, the crossovers made in *c(3)G^{ccΔ1}* heterozygotes
273 displayed an altered distribution along the length of the *X* chromosome, while *c(3)G^{ccΔ1}*
274 homozygotes severely reduced the frequency of crossing over on the *X*.

275 In WT, the majority of crossovers are known to occur in the middle one-third of the
276 chromosome arms and are inhibited near the centromeres and telomeres. Indeed, in the WT
277 control for our *X* chromosome recombination assay, most of the crossovers occurred between
278 the markers *vermillion* (*v*) and *forked* (*f*), which reside in the medial one-third of the *X*

279 chromosome (Fig 4A; Table 1 and S2). However, in *c(3)G*$^{cc\Delta 1}$ heterozygotes, the crossover
280 distribution was shifted toward the centromere-proximal region of the chromosome, such that
281 most crossovers occurred between the *forked* and *yellow*$^{+}$ (*y*$^{+}$) markers that encompass the
282 centromere. This crossover distribution shift resulted in a corresponding decrease in crossovers
283 in the distal chromosome regions, between the markers *scute* (*sc*) and *crossveinless* (*cv*). Also,
284 the overall map length of the *X* chromosome was slightly decreased in *c(3)G*$^{cc\Delta 1}$ heterozygotes
285 (51.2 cM in *c(3)G*$^{cc\Delta 1}$ heterozygotes vs. 63 cM in WT; Table 1). Thus, *c(3)G*$^{cc\Delta 1}$ heterozygotes
286 appear to alter the distribution of crossovers, without greatly changing the total number of
287 crossovers on the *X*.

288 In contrast, *c(3)G*$^{cc\Delta 1}$ homozygotes severely reduced crossing over on the *X*
289 chromosome (Fig 4A; Table 1). The total map length of the *X* chromosome decreased by more
290 than 80%, to 11.8 cM from 63.0 cM in WT, with the majority of the reduction in the medial and
291 distal intervals. However, even with this reduction the distribution of crossovers seems to
292 display the same centromere-proximal shift as in *c(3)G*$^{cc\Delta 1}$ heterozygotes.

293 A more comprehensive approach for understanding these reductions in exchange lies in
294 the application of Weinstein's method to calculate the frequency of bivalents that underwent
295 zero (E_0), one (E_1), or two (E_2) crossover events [36]. This method accounts for the fact that a
296 single recombination event between two homologs will produce two single crossover and two
297 noncrossover chromatids (only one of which is recovered) and that a double crossover event
298 (depending on whether it is a two-strand, a three-strand, or a four-strand double) will produce
299 some combination of noncrossover, single crossover, or double crossover chromatids (again,
300 only one of which is recovered). In WT, the frequency of noncrossover bivalents (or E_0
301 bivalents) was 18.9%, while in *c(3)G*$^{cc\Delta 1}$ homozygotes it was 79.2%—a four-fold increase in the
302 frequency of an oocyte receiving a noncrossover bivalent (Table 1). The remaining ~20% of *X*
303 chromosomal bivalents in *c(3)G*$^{cc\Delta 1}$ homozygotes did undergo a single crossover event, creating

304 single crossover (or E_1) bivalents and the vast majority of these single crossovers occurred in
305 centromere-proximal intervals (Fig 4A).

306 The presence of SC between homologous chromosomes is thought to keep them paired
307 throughout pachytene, which promotes crossing over between two homologous chromosomes.
308 Since the SC is prematurely disassembled in *c(3)G*^{ccΔ1}, it is possible that homologous
309 chromosome pairing may be lost before crossovers can be established, which may explain the
310 altered crossover distribution. We analyzed homolog pairing using euchromatic FISH probes at
311 distal (3C3–3C7) and proximal (15C1–15D6) regions on the *X* chromosome (Fig 4B; Table S2
312 and S3). A locus was considered paired if the distance between the two FISH probe foci was
313 less than 0.75 μm and unpaired if foci exhibited a distance 0.75 μm or greater.

314 In *c(3)G*^{ccΔ1} heterozygotes, both distal and proximal probes were paired in nearly 100%
315 of the oocytes in zygotene/early pachytene (region 2A) (Fig 4B, Table S3). However, the distal
316 probe was progressively less paired as the cells progressed to early pachytene (region 2B) and
317 mid pachytene (region 3). The proximal probe remained nearly 100% paired throughout these
318 regions. Thus, the centromere-proximal shift in recombination was correlated with a loss of
319 distal euchromatic pairing and a maintenance of proximal euchromatic pairing on the *X*
320 chromosome in *c(3)G*^{ccΔ1} heterozygotes.

321 Unlike *c(3)G*^{ccΔ1} heterozygotes, *c(3)G*^{ccΔ1} homozygotes displayed a progressive loss of
322 euchromatic pairing at both proximal and distal loci on the *X* chromosome, suggesting that the *X*
323 chromosomes may be unpaired by mid pachytene (Fig 4B, Table S3). Based on our FISH
324 assay, the proximal locus was able to maintain pairing more effectively than the locus detected
325 by the distal probe, which may explain why the few crossovers observed in *c(3)G*^{ccΔ1}
326 homozygotes occur in the centromere proximal region of the *X* chromosome. Indeed, we
327 propose that the loss of homolog pairing caused by a progressive loss of *X* chromosome SC is

328 the reason for the significant decrease in *X* recombination observed in *c(3)G*$^{cc\Delta 1}$ homozygotes. If
329 we are correct in this asserion, then the observation that homolog pairing is not drastically
330 reduced in *c(3)G*$^{cc\Delta 1}$ homozygotes until early pachytene (region 2B) suggests that crossover
331 designation on at least the *X* chromosome may be occurring either multiple times throughout
332 pachytene or later in pachytene than was previously thought.

333 **Autosomal crossover distribution is shifted to centromere-proximal regions**

334 Meiotic mutants that decrease recombination on the *X* chromosome also display similar
335 decreases in recombination on the autosomes [22, 27, 29, 37, 38]. It was therefore surprising
336 that both *c(3)G*$^{cc\Delta 1}$ homozygotes and heterozygotes displayed robust recombination on the
337 autosomes with the map lengths of each autosome increasing by more than 10 map units,
338 suggesting that each chromosome received more crossovers than normally would occur in WT
339 (Fig 4C,E; Tables 2 and 3). Indeed, to our knowledge, *c(3)G*$^{cc\Delta 1}$ is the first mutant in Drosophila
340 to exhibit such dramatic differences in terms of its effects on recombination on the *X*
341 chromosome compared to the autosomes. Moreover, the biological significance of finding that
342 the *X* chromosome may be more sensitive to *c(3)G*$^{cc\Delta 1}$-induced changes in the SC than the
343 autosomes may be that the various chromosome arms differ in their requirements for proper SC
344 structure and function.

345 Although overall recombination on the autosomes was robust, the crossover distribution
346 was shifted to the centromere-proximal regions in both *c(3)G*$^{cc\Delta 1}$ homozygotes and
347 heterozygotes. On the *3*rd chromosome, we observed a slight decrease in recombination in the
348 distal interval [*roughoid–hairy (ru–h*)] of both homozygotes and heterozygotes (Fig 4E; Table 3),
349 while on the *2*nd chromosome, only *c(3)G*$^{cc\Delta 1}$ homozygotes displayed a decrease in the distal
350 interval *net-decapentaplegic (net–dpp)* (Fig 4C; Table 2).

351 However, the most striking effects of the *c(3)G*^{ccΔ1} mutants on autosomal crossover
352 distribution can be seen by considering the intervals that span their centromeres (Fig 4C,E;
353 Tables 2, 3 and S2). On the *2*nd chromosome, exchange in the pericentromeric *purple* to
354 *cinnabar* (*pr–cn*) interval increased more than three fold in both heterozygotes and
355 homozygotes when compared to WT. Moreover, on the *3*rd chromosome, both *c(3)G*^{ccΔ1}
356 heterozygotes and homozygotes also showed a greater than 300% increase in recombination
357 frequency for the centromere spanning interval *scarlet* to *curled* (*st–cu*). Indeed, for the *3*rd
358 chromosome more than one third of the crossover events occurred in the pericentromeric *st–cu*
359 interval (as compared to 12% in wild type). Thus, both autosomes displayed a substantial
360 increase in pericentromeric recombination frequency compared to WT, suggesting that the
361 *c(3)G*^{ccΔ1} mutation may alleviate constraints that mediate recombination in such intervals, such
362 as centromere effect, which normally functions to restrict recombination in these intervals.

363 Since the *X* chromosome displayed both a centromere-proximal shift in recombination
364 and a premature loss in homolog pairing, we wondered if the discontinuous SC in *c(3)G*^{ccΔ1} was
365 affecting homolog pairing on the autosomes in a similar manner. In *c(3)G*^{ccΔ1} homozygotes,
366 these decreases in recombination were paralleled by progressive decreases in euchromatic
367 pairing for the distal probe on each autosome (Fig 4C–F; Tables 2, 3 and S3). Both the proximal
368 and medial probes remained relatively well paired on the autosomes throughout zygotene to
369 mid pachytene (region 2A to region 3) in *c(3)G*^{ccΔ1} homozygotes.

370 *c(3)G*^{ccΔ1} heterozygotes were able to maintain chromosome pairing along the entire
371 length of both the *2*nd and *3*rd chromosomes throughout zygotene to mid pachytene (region 2A to
372 region 3) (Fig 4D,F; Table S3). Because both *c(3)G*^{ccΔ1} homozygotes and heterozygotes
373 displayed the same altered crossover distribution, but only *c(3)G*^{ccΔ1} homozygotes lost pairing in
374 the distal chromosomal regions, the loss of homolog pairing in the distal regions of the
375 autosomes is likely not the cause of the centromere-proximal shift in crossing over. Rather, our

376 observations in *c(3)G*$^{cc\Delta 1}$ heterozygotes suggest that discontinuity of the SC may cause the shift
377 in crossover distribution. It is possible that because centromeric SC appears to be unaffected by
378 the *c(3)G*$^{cc\Delta 1}$ mutation, the SC near the centromeric heterochromatin is more stable, thus
379 making it more suitable for crossovers.

380

381 **_c(3)G_$^{cc\Delta 1}$ homozygotes and heterozygotes exhibit greatly reduced crossover interference**

382 It is known that intact SC is required for crossover interference, which acts to regulate the
383 number of crossovers formed on each chromosome arm by inhibiting crossovers from forming
384 within several megabases of each other [reviewed in 4, 31]. In other organisms, mutants that
385 display fragmented SC and/or chromosome axes have defects in crossover interference that
386 result in an increase in the number of crossovers [reviewed in 4]. On the *X* chromosome neither
387 *c(3)G*$^{cc\Delta 1}$ homozygotes nor heterozygotes displayed an increase in crossing over, in fact
388 *c(3)G*$^{cc\Delta 1}$ homozygotes caused a severe reduction in crossing over (Fig 4A). Thus, it is not
389 surprising that crossover interference is unaffected on the *X* chromosome in either *c(3)G*$^{cc\Delta 1}$
390 homozygotes or heterozygotes; but rather the observed loss of recombination is the result of a
391 loss of homolog pairing and/or synapsis (Table 1).

392 However, unlike the *X* chromosome, the autosomes displayed an increase in the
393 frequency of crossing over in *c(3)G*$^{cc\Delta 1}$ homozygotes and heterozygotes suggesting that
394 crossover interference may be affected (Fig 4C,E). Indeed, crossover interference is reduced in
395 *c(3)G*$^{cc\Delta 1}$ mutants on chromosome *2*. *c(3)G*$^{cc\Delta 1}$ heterozygotes have a complete or near complete
396 loss of crossover interference across the entire chromosome (Table 2). This decrease in
397 interference allows for an increase in the occurrence of double and triple crossovers (Table 2)
398 and results in an increase in map length [WT = 52.2 cM; *c(3)G*$^{cc\Delta 1}$ homozygotes = 67.6 cM;

399 *c(3)G*$^{cc\Delta 1}$ heterozygotes = 72.8 cM]. It is possible that the decreased interference on the *2*nd
400 chromosome results from the fragmented SC observed in the *c(3)G*$^{cc\Delta 1}$ mutants.

401 On chromosome *3, c(3)G*$^{cc\Delta 1}$ homozygotes displayed levels of crossover interference
402 similar to WT in the distal regions of the chromosomes (Table 3). However, in the centromere-
403 proximal regions [*thread/scarlet/curled* (*th/st/cu*)], the effect of interference seemed to get
404 significantly weaker (WT = –4.5; *c(3)G*$^{cc\Delta 1}$ homozygotes = –12.6). While we did not expect to
405 observe positive crossover interference across the centromere due to the centromere effect and
406 other potential factors functioning to suppress crossing over in this region, the large increase in
407 negative crossover interference was unexpected. Furthermore, this increase in negative
408 crossover interference may explain the observed increase in map length for *c(3)G*$^{cc\Delta 1}$
409 homozygotes on chromosome *3* (WT = 50.9 cM; *c(3)G*$^{cc\Delta 1}$ homozygotes = 59.6 cM). Curiously,
410 *c(3)G*$^{cc\Delta 1}$ heterozygotes displayed near-WT levels of crossover interference across all the
411 intervals assayed on chromosome *3* (Table 3). Thus, the observed increase in map length in
412 *c(3)G*$^{cc\Delta 1}$ heterozygotes cannot be explained by a loss in crossover interference (WT = 50.9 cM;
413 *c(3)G*$^{cc\Delta 1}$ heterozygotes = 63.8 cM).

414 **Chromosome segregation is unaffected by the *c(3)G*$^{cc\Delta 1}$ mutation**

415 It is well known that a decrease in recombination on the *X* chromosome should result in an
416 increase in frequency of *X* chromosome nondisjunction, such that the frequency of *X*
417 chromosome nondisjunction is equal to the frequency of E_0 cubed [39]. This reflects the
418 requirement for a pair of nonexchange autosomes to mediate missegregation of nonexchange *X*
419 chromosomes [40, 41]. Curiously, we did not observe this expected increase in the frequency of
420 *X* nondisjunction in *c(3)G*$^{cc\Delta 1}$ homozygotes (Table S4).

421 Moreover, mutants that decrease recombination on the *X* chromosome and increase the
422 frequency of *X* chromosome nondisjunction typically also decrease recombination on the

423 autosomes [37, 38]. However, *c(3)G*$^{cc\Delta 1}$ homozygotes showed robust recombination on the
424 autosomes (Fig 4). Previous studies have shown that the distributive system, which normally
425 functions to segregate the obligately achiasmate *4*th chromosomes, can accurately segregate
426 two achiasmate chromosomes, such as the *X* and *4*th chromosomes [41]. Therefore, in *c(3)G*$^{cc\Delta 1}$
427 homozygotes, it is likely that the lack of nondisjunction is due to the distributive system's ability
428 to accurately segregate the two achiasmate *X* and *4*th chromosomes. The mechanism of how
429 the distributive system accomplishes accurate segregation without a crossover is unclear, thus
430 future studies are needed to elucidate this mechanism.

431

432 **DISCUSSION**

433 Although our understanding of SC structure has been greatly facilitated by advancements in
434 superresolution microscopy, which have revealed a more precise three-dimensional model of
435 SC ultrastructure, there is still much to learn about SC function. The multiple roles the SC plays
436 during meiotic prophase illustrate the functional importance of this protein complex in ensuring
437 the successful transmission of genetic information from one generation to the next. However,
438 because the SC is integral for the proper execution of so many meiotic processes, it has been
439 difficult to elucidate which SC proteins or protein domains are required for which functions.
440 Here, we show that a deletion in the large coiled-coil domain of C(3)G reveals two different
441 requirements for the SC: first, the deleted coiled-coil region in *c(3)G*$^{cc\Delta 1}$ is required to maintain
442 both SC structure along the chromosome arms and homolog pairing during meiotic prophase;
443 and second, the SC's ability to facilitate recombination depends upon its full-length assembly. In
444 addition, each chromosome appears to respond differently, on both local and global levels, to
445 structural changes in the SC.

446 **Centromeric SC versus euchromatic SC**

447 The difference between the kinetics of SC assembly and disassembly along the chromosome
448 arms versus at the centromeres suggests that the SC at the centromeres might be structurally
449 different than the SC along the chromosome arms. Indeed, it is known that the SC at the
450 centromeres requires certain proteins that euchromatic SC does not. For example, the cohesion
451 complex proteins ORD, SUNN, and SOLO are required for assembly of centromeric SC but not
452 the assembly of euchromatic SC [42-45], while euchromatic—but not centromeric—SC requires
453 the LE protein C(2)M to completely synapse homologs [12]. We now show in *c(3)G*$^{cc\Delta 1}$ mutants
454 that a large region of the major coiled-coil domain in C(3)G is also dispensable for both
455 centromeric SC assembly and centromere clustering.

456 This difference between the SC at the euchromatin and at the centromere is not unique
457 to Drosophila. In yeast, the transverse filament protein Zip1 also persists long after the SC along
458 the chromosome arms has disassembled, and it is necessary for accurate achiasmate
459 chromosome segregation [46, 47]. Similarly, mice spermatocytes retain CR components of the
460 SC at the centromeres long after the SC has disassembled from the chromosome arms [48]. In
461 both mice and Drosophila, it is unclear why the SC persists at the centromeres, but it is possible
462 that centromeric SC in these organisms may function in achiasmate chromosome segregation,
463 as it does in yeast. Although errors in Drosophila female meiosis and mice spermatocytes are
464 rare, they do occur. Thus, persistence of centromeric SC may act as a backup segregation
465 mechanism to ensure proper chromosome segregation when a rare error does occur.

466 **Chromosome-specific regulation of recombination**

467 All previously characterized mutants in Drosophila that affect recombination on the *X*
468 chromosome show a similar, if not identical, effect on the autosomes. Prior to *c(3)G*$^{cc\Delta 1}$, all
469 known SC mutants abolished or severely reduced recombination on all three crossover
470 chromosomes [22, 24, 25, 27]. *c(3)G*$^{cc\Delta 1}$ is unique when compared to other SC mutants

471 because it differentially affects recombination on each chromosome, which suggests that each
472 chromosome has different rules for positioning crossovers along each chromosome arm [9].

473 While subtler than the differences observed between the *X* chromosome and the
474 autosomes, the differences between the two autosomes in *c(3)G*$^{cc\Delta 1}$ was indeed surprising.
475 Similar differences have been observed before. Miller et al. found that chromosome *2* displayed
476 a stronger effect of crossover interference than chromosome *3* [9]. They noticed that the *2*nd
477 chromosome rarely had double crossovers (out of 100 flies, only 14 double crossovers were
478 detected) and the double crossovers were positioned on average 11.5 Mb apart [9]. Meanwhile,
479 the *3*rd chromosome exhibited nearly twice as many double crossovers as the *2*nd chromosome
480 (out of 100 flies, 27 double crossovers were detected), and the double crossovers were
481 positioned on average 11.0 Mb apart [9, 49].

482 In *c(3)G*$^{cc\Delta 1}$ homozygotes and heterozygotes, both of the autosomes display defects in
483 crossover interference that result in an increase in the number of crossovers, but the *2*nd
484 chromosome seems to display a stronger effect. Perhaps this result is best interpreted in the
485 context of Miller et al.'s characterization of double crossovers on the two autosomes [9].
486 Because the *2*nd chromosome relies heavily on crossover interference to regulate crossing over,
487 a loss of crossover interference, like that observed in *c(3)G*$^{cc\Delta 1}$ homozygotes and
488 heterozygotes, would cause a large increase in the number of crossovers. Perhaps, then, the *3*rd
489 chromosome places more emphasis on an alternative mechanism, such as the centromere
490 effect, to regulate crossing over instead of crossover interference. This may explain why the
491 autosomes display subtle differences in recombination when crossover interference is
492 diminished to a similar degree in *c(3)G*$^{cc\Delta 1}$ homozygotes and heterozygotes.

493 Additionally, *c(3)G*$^{cc\Delta 1}$ demonstrates the importance of assaying multiple chromosomes
494 when mutants are defective in recombination. Although numerous previous characterizations of

495 recombination-defective mutants in Drosophila have only measured recombination on one
496 chromosome [16, 22, 24], our data from the *c(3)G*$^{cc\Delta 1}$ homozygotes illustrate how misleading it
497 can be to assay only one chromosome. In this case, the *X* chromosome is more sensitive to the
498 *c(3)G*$^{cc\Delta 1}$ mutation than are the autosomes. Differences between the sex chromosomes and the
499 autosomes are not specific to Drosophila. For example, studies in *Caenorhabditis elegans* found
500 that the *X* chromosome initiated meiotic DNA replication later than the autosomes [50, 51].
501 While the *X* chromosome and the autosomes seemed to homologously pair during the same
502 small window of time in *C. elegans*, complete synapsis of the *X* chromosome was delayed
503 and/or slower than the autosomes [50]. Currently, it is unknown in Drosophila if *X* chromosome
504 synapsis is delayed, but our data support a view that initiating a synapsis delay of the *X*
505 chromosome may result in a later initiation of recombination on the *X* chromosome.

506 Multiple factors work in concert to regulate recombination, and the SC appears to play a
507 vital role in this regulation. The SC is required for crossovers in all organisms that assemble the
508 structure, and *c(3)G*$^{cc\Delta 1}$ has demonstrated an additional role of the Drosophila SC in regulating
509 the positions of crossovers. Future studies are needed to determine the mechanism of how
510 C(3)G and the SC regulate recombination. Additionally, *c(3)G*$^{cc\Delta 1}$ is a large deletion mutant, thus
511 future experiments dissecting this deletion may reveal insights into this mechanism.

512

513 MATERIALS AND METHODS

514 Further information and requests for resources and reagents should be directed to and will be
515 fulfilled by the Lead Contact, R. Scott Hawley (RSH@stowers.org).

516 Experimental model and subject details

517 The Drosophila stocks used in the foregoing assays were kept at a humidity-controlled 25°C
518 and on standard food. All mention of "wild type" (WT) refers to the genotype: *y w; +/+; +/+; sv*$^{spa-}$
519 ^{pol}, unless stated otherwise. The key resource table contains a list of all the fly stocks used in
520 this manuscript.

521 *CRISPR/Cas9 generation of the c(3)G*$^{cc\Delta 1}$ *deletion flies*

522 To aid in screening for *c(3)G*$^{cc\Delta 1}$ mutant flies, we incorporated a piggy BAC transposon carrying
523 a 3xP3-DsRed that expresses in the fly eye into the intron directly downstream of the *c(3)G*$^{cc\Delta 1}$
524 deletion [intron 5 of *c(3)G*] in the homologous repair template plasmid. The piggy BAC
525 transposon plasmid was constructed to have flanking AarI and SapI restriction sites (Addgene
526 51434). We used PCR to obtain two fragments of *c(3)G* from the Drosophila genome that
527 flanked the position where the piggy BAC would be inserted and added in either an AarI or SapI
528 restriction site. The ~2600-bp fragment upstream of the piggy BAC insertion site contained AarI
529 sites and was obtained using these primers: Forward,
530 tataCACCTGCattaCCGAcgctagtggctcctagagttcag; Reverse,
531 gcagCACCTGCgcggTTAAtgaaaaagaatttataagtcttaccattaggttatc. The ~1000-bp fragment
532 downstream of the piggy BAC insertion site contained SapI sites and was obtained using these
533 primers: Forward, gccgGCTCTTCNTAAcctttttctacaaaatgatttatt; Reverse,
534 gtatGCTCTTCNCGGtcatcaaaacatagtttagtatcg.

535 To insert these fragments into the piggy BAC plasmid, the plasmid and the downstream
536 SapI-containing PCR was digested with SapI (also called LguI from ThermoFisher ER1931),
537 phosphatase treated (Antarctic phosphatase, NEB M0289S), and ligated together using T4
538 ligase (NEB M0202S). The upstream AarI-containing PCR fragment was TOPO cloned using
539 the Zero Blunt TOPO kit (ThermoFisher 451245). Then, TOPO AarI plasmid was cut using the
540 restriction enzyme HindIII (NEB R0104S), which removes a 708-bp fragment from *c(3)G*. The

541 cut TOPO AarI plasmid was then phosphatase treated and ligated back together to create the
542 *c(3)G*$^{cc\Delta 1}$ deletion. Then, this plasmid was digested with AarI (ThermoFisher ER1581) to
543 generate a ~1900-bp fragment containing the *c(3)G*$^{cc\Delta 1}$ deletion, which was cloned into the
544 piggy BAC plasmid containing the downstream SapI *c(3)G* fragment.

545 A CRISPR target sequence was selected from the flyCRISPR Optimal Target Finder
546 (http://tools.flycrispr.molbio.wisc.edu/targetFinder/). Only a single site upstream of the *c(3)G*$^{cc\Delta 1}$
547 deletion was selected (AAAGCTTTGTTGGCCTGTATTGG) and constructed into the pU6-BbsI-
548 chiRNA guide RNA (gRNA) plasmid (Addgene 45946). Sense
549 (CTTCGAAAGCTTTGTTGGCCTCTAT) and antisense (AAACATAGAGGCCAACAAAGCTTTC)
550 oligonucleotides were ordered from IDT and cloned into the gRNA plasmid as described by the
551 flyCRISPR subcloning pU6-gRNA protocol (http://flycrispr.molbio.wisc.edu/protocols/gRNA).
552 Three single nucleotide polymorphisms (SNPs) were made in the CRISPR target sequence (the
553 mutated bases are shown in bold: ccaataga**a**gc**g**aa**t**aaagcttt) in the *c(3)G*$^{cc\Delta 1}$ homologous repair
554 template plasmid to prevent Cas9 from cutting this plasmid. These SNPs were made using the
555 Quik Change II XL Site-Directed Mutagenesis Kit (Agilent Technology, 200521) and the reaction
556 was performed as described in the kit protocol. The gRNA and *c(3)G*$^{cc\Delta 1}$ homologous repair
557 template plasmid were sent to Genetivision (Houston, Texas) for injection into *y m[VASA-Cas9-*
558 *3xGFP]ZH-2A-3xRFP w*^{1118}*/FM7c* flies (BLM 51323). Genetivision injected the gRNA plasmid at
559 250 ng/µl and the *c(3)G*$^{cc\Delta 1}$ homologous repair template at 500 ng/µl.

560 *c(3)G*$^{cc\Delta 1}$ was isolated by crossing the G0 injected flies to *y w; Pr/TM3; sv*$^{spa\text{-}pol}$, then the
561 F1 progeny were screened for expression of dsRed in the fly eyes. Unfortunately, the genomic
562 locus marking the *VASA-Cas9* transgene is marked with RFP, so only F1 males were screened
563 for dsRed expression. PCR and Sanger sequencing were used to confirm the *c(3)G*$^{cc\Delta 1}$ deletion
564 and a transposase (BLM 32073) was crossed in to excise the transposon from the gene. Those
565 flies that successfully excised the transposon were PCR and Sanger sequenced to confirm the

566 absence of the transposon and presence of the *c(3)G*$^{cc\Delta 1}$ deletion. Then, the *c(3)G*$^{cc\Delta 1}$
567 chromosome was allowed to freely recombine with a multiply marked third chromosome to
568 remove any potential off-target mutations caused by removal of the piggy Bac and/or Cas9. Two
569 *c(3)G*$^{cc\Delta 1}$ fly stocks were established and used for all the assays in this manuscript: (1) carrying
570 all the markers from *3L* [*roughoid (ru), hairy (h), thread (th), scarlet (st)]* and two markers from
571 *3R [curled (cu), claret (ca)]* in addition to the *c(3)G*$^{cc\Delta 1}$ deletion, and (2) only carrying *ca* with the
572 *c(3)G*$^{cc\Delta 1}$ deletion.

573 **Method details**

574 *Immunohistochemistry for DeltaVision and STORM microscopy*

575 Ovary fixation and immunofluorescence for DeltaVision imaging were performed as detailed in
576 Lake et al. 2015 [29]. Briefly, ovaries were dissected in PBS with 10% Tween (PBST) for 15 min
577 and fixed in a 2% formaldehyde solution with heptane [165 µl PBS, 10 µl nonidet-P40 (Sigma-
578 Aldrich, 11332473001), 600 µl heptane and 25 µl of a 16% formaldehyde (Electron Microscopy
579 Sciences, 15710)] for 20 min. Then, ovaries were washed 3 times for 10 min each with PBST.
580 For experiments when only the early stages of oogenesis (stages 1–6) were analyzed, the
581 ovaries were clipped to remove the later stages of oogenesis. However, for the experiments
582 analyzing stages 7–9, the ovaries were rapidly pipetted to separate out the stages. Next,
583 ovaries were blocked in PBST+0.1% bovine serum albumin (BSA) for at least 1 hr, the block
584 was removed, and fresh PBST was added with the primary antibodies and left rocking overnight
585 at 4ºC. Primary antibodies used in this manuscript include mouse anti-C(3)G C-terminus (1A8–
586 1G2; used at 1:500; [23]), affinity-purified rabbit anti-Corolla (used a 1:2000; [24]), rat anti-CID
587 (used at 1:3000; from Claudio Sunkel), and mouse anti-γH2AV (used at 1:500; Iowa Hybridoma
588 Bank, UNC93-5.2.1; [30]). The next day, the primary antibodies were removed and the ovaries
589 were washed 3 times for 15 min each with PBST. Then, secondary antibodies were added in

590 PBST and incubated for 2 hr, rocking at room temperature. All secondary antibodies were used
591 at 1:500, and the secondary antibodies used were Alexa Fluor 488 goat anti-mouse
592 (ThermoFisher, A11001), Alexa Fluor 555 goat anti-mouse (ThermoFisher, A21422), Alexa
593 Fluor 647 goat anti-mouse (ThermoFisher, A21235), Alexa Fluor 488 goat anti-rabbit
594 (ThermoFisher, A11008), Alexa Fluor 555 goat anti-rabbit (ThermoFisher, A21428), Alexa Fluor
595 647 goat anti-rat (ThermoFisher, A21434), and Alexa Fluor 555 goat anti-rat (ThermoFisher,
596 A21247). After 1 hr and 45 min, 5 µl of 100X 4'6-diamididino-2-phenylindole (DAPI) was added
597 and left to incubate with the secondaries for 15 min. Ovaries were then washed with PBST 3
598 times for 15 min and mounted in Prolong Gold (Life Technologies, P36930) using an NA 1.5
599 glass coverslip and frosted glass slides.

600 For STORM of C(3)G, ovary fixation and immunofluorescence was performed as
601 described above with minor changes. The primary antibody was a mouse monoclonal anti-
602 C(3)G C-terminal (1A8–1G2, used at 1:500, [23]) and the secondary antibody was Alexa Fluor
603 647 mouse (used at 1:500; ThermoFisher, A21235). Since samples had to be imaged the same
604 day they were mounted, secondary antibody incubation was left rocking on the nutator overnight
605 at 4ºC. Then, the sample was washed 2 times in PBST for 15 min each. No DAPI was added to
606 these samples. Following the washes, the sample was optically cleared using 2,2-thiodiethanol
607 (TDE; VWR, 700008-210). The sample was rocked on the nutator at room temperature for 10
608 min each in 10% TDE in PBS, followed by 20% TDE in PBS, and finally in 50% TDE in PBS. For
609 mounting, a mixture of TDE and VECTASHIELD (VWR, 101098-042) was used since it had
610 been shown that low concentrations of VECTASHIELD allowed for blinking of the Alexa Fluor
611 647 dye [52]. We found that for WT samples, a mixture of 91%TDE/9% VECTASHIELD resulted
612 in robust blinking of the dye and higher VECTASHIELD concentrations stabilized the dye,
613 preventing it from blinking. In *c(3)G*$^{cc\Delta 1}$ homozygotes and heterozygotes, we had to increase the
614 concentration of VECTASHIELD to obtain the same robust blinking as WT, thus these samples

615 were mounted in 88%TDE/12% VECTASHIELD. All samples were mounted with NA1.5
616 coverslips on glass slides and sealed using clear nail polish for STORM imaging that same day.

617 *Fluorescent BAC probes for fluorescent in situ hybridization (FISH)*

618 FISH probes were designed from bacterial artificial chromosomes (BACs) obtained from the
619 Children's Hospital Oakland Research Institute (CHORI;
620 http://bacpacresources.org/library.php?id=30). The following BACs were used: for *2L* RP98-
621 28O9 (polytene band 22A2-22A4), RP98-43K24 (polytene band 32E2-32F2), RP98-7D17
622 (polytene band 38E4-38F4); for *3L* RP98-2N23 (polytene band 61D-61E), RP98-26C20
623 (polytene band 69B1-69C2), RP98-3J2 (polytene band 77F5-78B1); for the *X* RP98-3D13
624 (polytene band 3C3-3C7), RP98-9H1 (polytene band 15C1-15D6).

625 Bacteria containing each BAC were grown on LB+chloramphenicol and the BACs were
626 isolated using a modification of the QIAGEN Plasmid Midi Kit protocol (QIAGEN, 12143). A
627 single bacteria colony was grown in 5 mL LB+chloramphenicol for 6–8 hours, then that culture
628 was moved into 100 mL culture of LB+chloramphenicol and grown overnight. Next, cells were
629 spun down in two 50-mL bottles at 4500 g for 20 min at 4°C and the supernatant was removed
630 (Note: Can stop here and freeze cells at 80°C.) The pellets were resuspended in 10 mL Buffer
631 P1 followed by adding 10 mL Buffer P2 to each bottle and gently mixed by inverting 4–6 times.
632 Then, the tubes were incubated at room temp for 5 min. Chilled Buffer P3, 10 ml, was added to
633 each tube and immediately mixed by gently inverting 4–6 times. The tubes were incubated on
634 ice for 15 min. The lysed cells were centrifuged at ≥ 20,000 g for 30 min at 4°C (JA-20 rotor) and
635 the supernatant was moved to a new tube followed by centrifugation at ≥ 20,000g for 15 min at
636 4°C (JA-20 rotor). The QIAGEN-tip 100 were equilibrated by applying 4 mL Buffer QBT and
637 allowed to flow through the column by gravity. The two supernatants were pooled together and
638 added to the QIAGEN-tip column allowing gravity flow to run the liquid through the column. The

639 QIAGEN-tip column was washed twice with 10 mL Buffer QC and the BACs were eluted off the
640 column with 5 mL Buffer QF pre-warmed to 65°C. Following elution, the DNA was precipitated
641 by adding 3.5 mL isopropanol, mixed well, and centrifuged at ≥ 15,000g for 30 min at 4°C (JA-
642 20 rotor). The DNA pellet was washed with 2 mL 70% ethanol and centrifuged at ≥ 15,000g for
643 10 min, then allowed to air dry for 5–10 min. The DNA was dissolved in 50 µl of water, and
644 additional water may need to be added to solubilize all the DNA.

645 To make the FISH probes, the BACs were PCR amplified using the Illustra GenomiPhi
646 V2 DNA Amplification Kit (GE 25-6600-30). The concentration of the BAC DNA was determined
647 using the Quibit and 10 ng of BAC DNA was used for one amplification reaction. The
648 amplification reaction was performed as described in the kit protocol. To confirm that the
649 amplification reaction worked, each sample was run on a DNA agarose gel to display a bright
650 smear ranging from ≥10 kb–3 kb DNA sized fragments. Also, the Qubit dsDNA HS assay kit
651 protocol (ThermoFisher, Q32851) was used to confirm that each amplification reaction had ~4–
652 7 ng of DNA.

653 Next, the amplified BAC was restriction enzyme digested using AluI (NEB R137S), HaeII
654 (NEB R107S), MseI (NEB R0525S), RsaI (NEB R0167S), MboI (NEB R0147S) and MspI (NEB
655 R0106S). A 100-µl digestion reaction was set up adding in all 20 µl of the amplified BAC DNA,
656 64.5 µl of the New England BioLabs smart cut buffer, and 1 µl of each restriction enzyme (for
657 Msp1, only 0.5 µl was added). The digestion reaction was left overnight at 37ºC in a
658 thermocycler. Complete digestion of the BAC DNA was checked on a DNA agarose gel where
659 most of the DNA fragments should be below the 500-bp DNA size marker. Following the
660 digestion, the DNA was precipitated using 2.5 volumes 100% ethanol, 1/10 volume 3M sodium
661 acetate, and 1 µl of 20 mg/mL glycogen (ThermoFisher, 10814010). The precipitated DNA was
662 washed using 70% ethanol and resuspended in 50–60 µl of the labeling buffer from the ULYSIS
663 Nucleic Acid Labeling Kits (ThermoFisher – AF647 kit, U21660; AF546 kit, U21652).

664 To label the DNA with AF647 or AF546, the ULYSIS Nucleic Acid Labeling Kits were
665 used. For labeling, we used 10 µl of the digested BAC DNA and followed the protocol provided
666 in the ULYSIS kits. We removed the unreacted dyes from the labeling reaction using Centri-Sep
667 Columns (Princeton Separation, CS-900). The protocol provided with the columns was used to
668 remove the unreacted dyes, thereby isolating the fluorescently labeled BAC probes. The
669 resulting labeled BAC DNA was stored at –20ºC.

670 *Fluorescent in situ hybridization of ovaries*

671 Ovaries were dissected in PBST and fixed in a 3.7% formaldehyde and sodium cacodylate
672 solution. A 2X fix buffer (200 mM sodium cacodylate pH7.2, 200 mM sucrose, 80 mM sodium
673 acetate, 20 mM EGTA) was made in advance and stored in 500-µl aliquots at –20ºC. The 1X fix
674 solution (500 µl 2X Fix buffer, 232 µl 16% formaldehyde, 268 µl sterile water) was made
675 immediately prior to dissecting the ovaries and each ovary sample was fixed in 500 µl of the 1X
676 fix solution. Ovaries were fixed for 4 min rocking on the nutator at room temperature. Then, the
677 ovaries were rinsed three times in 2X Saline Sodium Citrate buffer with 0.1% Tween-20 (SCCT)
678 for 10 min each. Next, the ovary tips were clipped off using forceps to help isolate the
679 germarium from the later stages of oogenesis. These tips were transferred into new thin-walled
680 0.5-mL tubes and stepped into 2X SCCT with 50% formamide by sequentially adding each
681 formamide solution for 10 min each while nutating. First, the tips were incubated in 500 µl of a
682 2X SCCT with 20% formamide, then 2X SCCT with 40% formamide, and finally 2X SCCT with
683 50% formamide. The previous 2X SCCT with 50% formamide was removed and replaced with
684 fresh 2X SCCT with 50% formamide that was then incubated in a thermocycler at 37ºC for 1–2
685 hr.

686 Following that incubation, the 2X SCCT with 50% formamide was removed and the
687 hybridization mixture was added to the ovary tips. For all the BAC probes, the hybridization

688 mixture contained 2 µl BAC probe labeled with AF647, 2 µl BAC probe labeled with AF546, and
689 36 µl 1.1X hybridization solution (1.0 g dextran sulfate, 1.5 mL 20X SSC, 5 mL formamide,
690 water up to 9 ml; made in advance and stored at 4ºC). In a thermocycler, the probes and
691 chromosomal DNA were denatured for 2 min at 91ºC, then hybridized overnight at 37ºC.

692 The following day 500 µl 2X SCCT with 50% formamide was added to the hybridization
693 mixture and left at 37ºC to settle. Then, the solution was removed and the ovaries were washed
694 with 2X SCCT with 50% formamide three times at 37ºC for 20 min each. Next, the ovary tips
695 were exchanged back into 2X SCCT without formamide while nutating at room temperature by
696 adding 2X SCCT with 40% formamide for 10 min and then adding 2X SCCT with 20%
697 formamide for 10 min. The ovaries were washed once with 2X SCCT for 10 min, then washed
698 two more times with PBST for 10 min each. Then, block [1% Fraction V BSA in PBST] was
699 added and ovary tips were incubated for 1 hr at room temperature on the nutator. The block was
700 removed and primary antibodies were added in PBST and incubated overnight at 4ºC on the
701 nutator. For all FISH samples, a cocktail of three mouse monoclonal anti-C(3)G C-terminal
702 antibodies (1A8–1G2, 5G4–1F1, 1G5–2F7; [23]) was added and each antibody was used at a
703 dilution of 1:500.

704 Ovary tips were washed three times for 20 min each in PBST and the Alexa Fluor 488
705 mouse secondary was added at a dilution of 1:500. The secondary antibody was incubated for 2
706 hr rocking at room temperature. Then, 5 µl of 100X DAPI was added and incubated for an
707 additional 10 min. Next, the ovary tips were washed three times for 20 min each in PBST and
708 mounted onto glass slides with NA1.5 coverslips in Prolong Gold. After 24 hr the slides were
709 sealed using clear nail polish and kept at 4ºC prior to imaging on the DeltaVison.

710 *DeltaVision and STORM microscopy*

711 Except for the STORM imaging (see below), all images were acquired on an inverted
712 DeltaVision microscopy system (GE Healthcare) with an Olympus 100x Objective (UPlanSApo
713 100x NA 1.40) and a high-resolution CCD camera. The images from the DeltaVision were
714 deconvolved using SoftWorRx v. 6.5 software following the GE healthcare protocol. Images
715 were cropped and brightness and contrast was slightly adjusted using ImageJ.

716 STORM Imaging was performed on an OMX V4 microscopy system (GE healthcare)
717 with an Olympus 60x TIRF Objective (APO N 60x NA 1.49). Alexa Fluor 647 was continuously
718 excited with a 642 nm laser without UV activation, and the emission photons were filtered using
719 a band-pass emission filter (679/41, Semrock) and collected by a PCO-Edge sCMOS camera
720 with an 80-nm pixel size. Laser intensity measured after the objective was 4–6 kW/cm-2.
721 16,000–20,000 frames were recorded for each STORM data with 12–15 ms exposure time
722 depending on signal intensity.

723 *Meiotic recombination*

724 The multiply-marked *X* chromosome (*y sc cv v f* y^+) used in all the *X* recombination assays
725 carries two versions of the yellow gene: (1) a mutant version of the yellow gene at the genomic
726 locus on the tip of the long arm of the *X* chromosome (represented as *y*) and (2) a wild type
727 copy of the yellow gene that was integrated onto the short arm of the *X* chromosome on other
728 side of the centromere (represented as y^+). To assay the frequency of recombination on the *X*
729 chromosome in *c(3)G*^{ccΔ1} homozygotes, males of the genotype w^+*/BsY; mm c(3)G*^{ccΔ1}*/TM3;*
730 *sv*$^{spa\text{-}pol}$/+ were crossed to *FM7w/y sc cv v f* y^+*; D/TM3* virgin females. The *y sc cv v f* y^+*/BsY; mm*
731 *c(3)G*^{ccΔ1}*/+; sv*$^{spa\text{-}pol}$/+ male progeny from this cross were then crossed to w^+*/y w; mm*
732 *c(3)G*^{ccΔ1}*/TM3; sv*$^{spa\text{-}pol}$/+ virgin females, which generated females carrying *y sc cv v f* y^+*/y w; mm*
733 *c(3)G*^{ccΔ1}*; sv*$^{spa\text{-}pol}$/+. These females were crossed individually to *y sc cv v f* y^+*/BsY* males and the
734 female progeny were scored for the presence of the *sc, cv, v, f* and y^+ markers to determine the

735 *X* recombination frequency. *c(3)G*$^{cc\Delta 1}$ heterozygotes were generated by crossing males of the
736 genotype *y w/BsY; mm c(3)G*$^{cc\Delta 1}$*/TM3; sv*$^{spa\text{-}pol}$/+ to *FM7w/y sc cv v f y*$^{+}$ virgin females. The
737 resulting female progeny of the genotype *y sc cv v f y*$^{+}$*/y w; mm c(3)G*$^{cc\Delta 1}$/+; *sv*$^{spa\text{-}pol}$/+ were
738 individually crossed to *y sc cv v f y*$^{+}$*/BsY* males. The *X* recombination frequency was determined
739 by scoring the female progeny for the presence of *sc, cv, v, f* and *y*$^{+}$ markers. To assay *X*
740 recombination in WT, *y w; sv*$^{spa\text{-}pol}$ virgin females were crossed to *y sc cv v f y*$^{+}$*/BsY* males. The
741 virgin female progeny from this cross were individually crossed to *y sc cv v f y*$^{+}$*/BsY* males. The
742 *X* recombination frequency was determined by scoring the female progeny for the presence of
743 *sc, cv, v, f* and *y*$^{+}$ markers.

744 To assay recombination frequency along the *2*nd chromosome in *c(3)G*$^{cc\Delta 1}$ homozygotes,
745 virgin females of the genotype *y w; +/+; c(3)G*$^{cc\Delta 1}$ *ca; sv*$^{spa\text{-}pol}$ were crossed to *w/y; net dpp dpy b*
746 *pr cn/cyo; mm c(3)G*$^{cc\Delta 1}$*/TM3; sv*$^{spa\text{-}pol}$/+ males. Single virgin female progeny of the genotype
747 *yw/w; net dpp dpy b pr cn/+; mm c(3)G*$^{cc\Delta 1}$*/ c(3)G*$^{cc\Delta 1}$ *ca; sv*$^{spa\text{-}pol}$/+ were crossed to *w*$^{+}$*/y; net dpp*
748 *dpy b pr cn* males. The recombination frequency was determined by scoring the female progeny
749 for the presence of *net, dpp, dpy, b, pr,* and *cn* markers. To assay recombination frequency
750 along the *2*nd chromosome in *c(3)G*$^{cc\Delta 1}$ heterozygotes, virgin WT females were crossed to *w/y;*
751 *net dpp dpy b pr cn/cyo; mm c(3)G*$^{cc\Delta 1}$*/TM3; sv*$^{spa\text{-}pol}$/+ males. Single virgin female progeny of the
752 genotype *yw/w; net dpp dpy b pr cn/+; mm c(3)G*$^{cc\Delta 1}$/+; *sv*$^{spa\text{-}pol}$/+ were crossed to *w*$^{+}$*/y; net dpp*
753 *dpy b pr cn* males. The recombination frequency was determined by scoring the female progeny
754 for the presence of *net, dpp, dpy, b, pr,* and *cn* markers. Lastly, to assay recombination
755 frequency along the *2*nd chromosome in wild type, virgin WT females (*y w; sv*$^{spa\text{-}pol}$) were crossed
756 to *w*$^{+}$*/y; net dpp dpy b pr cn* males. Single virgin female progeny of this cross were then crossed
757 to *w*$^{+}$*/y; net dpp dpy b pr cn* males. The *2*nd recombination frequency was determined by scoring
758 the female progeny for the presence of *net, dpp, dpy, b, pr,* and *cn* markers.

759 To assay recombination frequency along the *3rd* chromosome in *c(3)G^{ccΔ1}* homozygotes,
760 virgin females of the genotype *y w/w^{+}; mm c(3)G^{ccΔ1}/TM3; sv$^{spa-pol}$*/+ were crossed to *y w;*
761 *c(3)G^{ccΔ1} ca; sv$^{spa-pol}$* males. Single virgin female progeny of this cross that were homozygous for
762 the *c(3)G^{ccΔ1}* deletion were then crossed to *ru h th st cu sr e ca* males. The recombination
763 frequency was determined by scoring for the presence of *ru, h, th, st,* and *cu* in female progeny.
764 To assay recombination frequency along the 3rd chromosome in *c(3)G^{ccΔ1}* heterozygotes, virgin
765 wild type females were crossed to *y w/w^{+}; mm c(3)G^{ccΔ1}; sv$^{spa-pol}$*/+ males. Single virgin female
766 progeny of this cross were then crossed to *ru h th st cu sr e ca* males. The recombination
767 frequency was determined by scoring for the presence of *ru, h, th, st,* and *cu* in female progeny.
768 Lastly, to assay recombination frequency along the *3rd* chromosome in WT, virgin WT females (*y*
769 *w; sv$^{spa-pol}$*) were crossed to *ru h th st cu sr e ca* males. Single virgin female progeny of this
770 cross were then crossed to *ru h th st cu sr e ca* males. The recombination frequency was
771 determined by scoring for the presence of *ru, h, th, st,* and *cu* in female progeny.

772 *Meiotic nondisjunction*

773 For the *X* and *4th* chromosome nondisjunction assay, we introduced *y w* marked X
774 chromosomes and *sv$^{spa-pol}$* marked *4th* chromosomes into the *c(3)G^{ccΔ1} ca/TM3* stock to create a
775 *y w/y^{+}Y*; *c(3)G^{ccΔ1}/TM3; sv$^{spa-pol}$* stock. This was done by crossing males from *y w/y^{+}Y; Pr/TM3;*
776 *sv$^{spa-pol}$* to the *c(3)G^{ccΔ1}/TM3* stock. All nondisjunction assays were performed using the *y w/y^{+}Y*;
777 *c(3)G^{ccΔ1}/TM3; sv$^{spa-pol}$* stock. *X* and *4th* chromosome nondisjunction was assayed by crossing
778 virgin *y w; c(3)G^{ccΔ1}; sv$^{spa-pol}$* and *y w; c(3)G^{ccΔ1}/+; sv$^{spa-pol}$* females to *attached-XY, y^{+} v f B;*
779 *C(4)RM, ci ey^{R}* males, as described in Harris et al. 2003 (the *attached-XY* symbol represents the
780 chromosome *C(1;Y), IN(1)EN*, which is arranged as such *Y^{s}X•Y^{L}*) [53]. Virgin homozygous
781 females for *c(3)G^{ccΔ1}* were collected from the *y w/y^{+}Y*; *c(3)G^{ccΔ1}/TM3; sv$^{spa-pol}$* stock. Virgin
782 heterozygous *c(3)G^{ccΔ1}* females were created by crossing *y w/ y^{+}Y*; *c(3)G^{ccΔ1}/TM3; sv$^{spa-pol}$*

783 males to *y w; sv*$^{spa\text{-}pol}$ virgin females and collecting the virgin female progeny that displayed the
784 correct genotype (*y w*; *c(3)G*$^{cc\Delta 1}$*/+; sv*$^{spa\text{-}pol}$).

785 In this assay, *X* chromosome nondisjunction at meiosis I will result in yellow white (*y w*)
786 females, which are created by having the two maternal *X* chromosomes segregate to the same
787 pole (also known as a diplo-*X* ova), or yellow-plus vermillion forked Bar (y^+ *v f Bar)* males, which
788 are created by the segregation of none of the maternal *X* chromosomes into the egg, resulting in
789 an *attached-XY/0* male (also known as a nullo-*X* ova). Meiosis II nondisjunction is extremely
790 rare and using this assay as described above, the meiosis II nondisjunctional progeny will
791 phenocopy the meiosis I nondisjunctional progeny. Since *c(3)G*$^{cc\Delta 1}$ mutants display no
792 nondisjunction, we did not assay for meiosis II nondisjunction.

793 *4*th chromosome nondisjunction at meiosis I will result in sparkling poliert (*sv*$^{spa\text{-}pol}$)
794 progeny, which are created by having the two maternal *4*th chromosomes segregate to the same
795 pole (also known as a diplo-*4* ova), or cubitus interruptus eyeless Russian (*ci ey)* progeny,
796 which are created by the segregation of none of the maternal *4*th chromosomes into the egg,
797 resulting in a *C(4)RM/0* progeny (also known as a nullo-*4* ova). While rare, flies with four *4*th
798 chromosomes are viable and indistinguishable from regular progeny.

799 **Quantification and statistical analysis**

800 *γH2AV, CID, and SC intensity quantifications*

801 Oocyte staging for the γH2AV and CID quantifications was done according to Matthies et al.
802 [54]. Briefly, the germarium was identified by DAPI staining and each region was defined by the
803 pattern of SC staining. Region 2A contains at least 4 cells of the 16-cell cyst with either partially
804 or fully assembled SC, and in region 2B only 2 cells contain full-length SC. Region 3 (stage 1) is
805 at the base of the germarium where only 1 cell has full-length SC and the other cell has either
806 fully disassembled or is in the process of disassembling the SC. The rest of the stages (stage

807 2–9) were defined by measuring the size of the oocyte. Stage 2 is 25x25 μm, stage 3 is 35x35
808 μm, stage 4 is 40x50 μm, stage 5 is 55x75 μm, stage 6 is 60x85 μm, and stage 7 is 70x115 μm.
809 Each oocyte was measured using the SoftWoRx software, then classified as the stage to which
810 it was the closest in size. For stages 8 and 9 there is no quantitative way to measure the egg to
811 determine these stages. Instead, stage 8 is defined by being bigger than a stage 7 with the
812 oocyte cytoplasm occupying less than one-third of the egg. Stage 9 is defined by the oocyte
813 cytoplasm occupying one-third of the egg and the follicle cells beginning to migrate over the
814 oocyte.

815 Prior to the quantification of γH2AV and CID foci, individual nuclei from each region and
816 stage were 3D-cropped in ImageJ (NIH open source software). The number of foci present for
817 both γH2AV and CID foci was determined by analyzing each cropped nucleus in 3D and
818 counting the number of foci. N value for both γH2AV and CID data sets represents the number
819 of nuclei scored in each stage. In the germarium, more nuclei can be scored in region 2A than in
820 region 2B and region 3, thus the number of germaria analyzed varies accordingly, such that the
821 total nuclei scored in each region was 30. The analysis of region 2A came from 4–7 individual
822 germaria. The analysis of region 2B came from 13–19 individual germarium. The analysis of
823 region 3 came from 30 individual germaria. A Wilcoxon rank sum test was used for the P-value
824 calculation of the γH2AV data.

825 To estimate protein density at different stages for the mutants acquired here, we
826 performed quantitative imaging of the SC antibody Corolla labeled with Alexa Fluor 488. For this
827 analysis, we assumed that the antibody penetration and epitope availability was the same
828 between each of the regions/stages and for each mutant analyzed. SC intensity measurements
829 were obtained by performing sum projections over SC regions and then measuring the
830 integrated intensity of the sum projected region after subtracting the average intensity from a
831 manually selected region near each individual SC. In some cases, the exposure time and laser

832 power were changed in order to obtain reasonable images of low-intensity SCs. In those cases,
833 the intensity values were corrected to account for these changes.

834 *Euchromatic FISH pairing quantification*

835 The same staging of the germarium as described above was done for the quantification of the
836 euchromatic FISH pairing. To measure the distance between the FISH probe foci, a custom
837 ImageJ plug-in was used. First, the two FISH probe foci were selected as points using the
838 points tool and the coordinates of each point were recorded in the ROI manager. Then, the
839 plugin measure "3D jru v1" was run to calculate the 3D distance (in μm) between ROI point one
840 and ROI point two (available at http://research.stowers.org/imagejplugins). A slice spacing of
841 0.20 and pixel spacing of 0.06370 were used in the plugin to calculate the 3D distance between
842 the foci. A locus was considered paired if the distance between the FISH probe foci was <0.75
843 μm and unpaired if the distanced between the FISH probe foci was ≥0.75 μm. The n value for
844 this data is the number of nuclei scored. Similar to the γH2AV and CID quantification, the
845 number of germaria scored for region 2A, region 2B, and region 3 vary because the number of
846 quantifiable nuclei in each region varies. For all the probes assayed, on average ~4 germaria
847 were scored for region 2A, ~8 germaria were scored for region 2B, and ~13 germaria were
848 scored for region 3.

849 *STORM quantification*

850 STORM data was analyzed through an open source ImageJ plug-in [55]. Briefly, the acquired
851 image was smoothed by a Gaussian filter, and then each blinking molecule was fitted to a
852 Gaussian function by maximum likelihood fitting. Individual molecule's position, photon counts
853 and fitting standard deviation were stored for future processing. To correct and optimize the
854 results of the analysis, only molecules having 1–16 nm localization precision and 80–160 nm

855 fitting standard deviation were chosen for rendering and quantification. Cross-correlation
856 between subsets (~2000 frames) of localized molecules was calculated to correct lateral drift.

857 Measurements were performed using ImageJ and the following custom plugins:
858 fit_multi_gaussian_jru_v4; set_multi_plot_offsets_jru_v1; resample_plot_jru_v1;
859 normalize_trajectories_jru_v1; average_trajectories_jru_v1 (available at
860 http://research.stowers.org/imagejplugins). Measurements were performed on raw molecule
861 position accumulation images. Intensity (i.e. molecule position accumulation) profiles were then
862 averaged over a five-pixel-wide stripe perpendicular to the paired C(3)G C-terminal tracks.
863 Profile fits to double Gaussian functions were used to determine the centers of each profile.
864 Profiles were then realigned to these centers, normalized, and averaged to obtain the final
865 averaged histograms as described in [21]. This averaged profile was then fit to a double
866 Gaussian function, by nonlinear least squares as described in [56], using the open source tools
867 described above. Error analysis of the fit parameters was performed using a Monte Carlo
868 approach with 100 random simulations (also described in [56]). For wild type, n=26 SC
869 measurements; for *c(3)G*$^{cc\Delta 1}$ heterozygotes, n = 34 SC measurements; and for *c(3)G*$^{cc\Delta 1}$
870 homozygotes, n = 32 SC measurements. Standard t-test was used for statistical comparisons
871 between the *c(3)G*$^{cc\Delta 1}$ mutants and WT.

872 *Meiotic recombination quantification*

873 N values for the recombination assay refer to the number of progeny scored in each genotype.
874 For all the chromosomes assayed, map length was determined by dividing the number of
875 progeny that had a crossover between a given set of markers by the total number of progeny
876 scored for one genotype on a specific chromosome. For example, the map length from *sc-cv*
877 was determined by dividing the number of progeny that had a crossover between *sc-cv* markers
878 by the total number of *X* chromosome recombinant progeny scored for a specific genotype.

879 Interference was calculated by: $1 - \frac{observed\ double\ crossvers\ between\ adjacent\ intervals}{expected\ double\ crossovers\ between\ adjacent\ intervals}$

880 The number of expected double crossovers occurring in adjacent intervals was determined from
881 the WT recombination data by multiplying the map length of one interval by the map length of
882 the adjacent interval and then multiplying by the total number of recombinants scored. For
883 example, on the *X* chromosome the expected number of double crossovers occurring between
884 the *sc-cv* and *cv-v* intervals was calculated by:

885 $$\frac{sc{-}cv\ recombinants}{total\ X\ recombinants} \times \frac{cv{-}v\ recombinants}{total\ X\ recombinants} \times total\ X\ recombinants$$

886 The number of observed double crossovers between adjacent intervals was empirically
887 determined from the raw data. The total number of noncrossovers (NCOs), single crossovers
888 (SCOs), double crossovers (DCOs), triple crossovers (TCOs) and quad crossovers (QCOs)
889 were empirically determined from the raw data. Exchange rank was determined according to the
890 method in Weinstein [36, 57].

891 *Meiotic nondisjunction quantification*

892 For both the *X* and *4*th chromosomes, half of the progeny from the nondisjunction assay are
893 inviable. Diplo-*X* ova are only viable when fertilized with sperm not carrying the *attached-XY*. If
894 these ova are fertilized with sperm carrying the *attached-XY,* the resulting progeny will be
895 *XX/attached-XY*, which is inviable. Nullo-*X* ova are only viable when fertilized with sperm
896 carrying the *attached-XY*. If these ova are fertilized with sperm not carrying the *attached-XY*, the
897 resulting progeny will not have any sex chromosomes, which is inviable. Since only half of the
898 nondisjunctional progeny are recovered, we adjusted the total by doubling the number of *X*
899 chromosome nondisjuctional progeny.

900 Nullo-*4* flies, from nullo-*4* ova fertilized by nullo-*4* sperm, are not able to survive.
901 Additionally, haplo-*4 minute* flies (or a single *4/0*) will occur as regular progeny from the cross,

902 but these flies are very poor and recorded but not scored in the nondisjunction tables. If both the
903 *X* and *4*th chromosomes nondisjoin together (*X–4*) only two of the four possible progeny are
904 viable. Thus, we adjusted the total by doubling the number of the *X–4* nondisjunctional progeny.
905 For both *X* and *4,* the frequency of nondisjunction was calculated as described in Hawley et al.
906 1992 [40].

907 **Data and software availability**

908 Primary data files for the figures in this paper are publicly accessible
909 at www.stowers.org/research/publications/odr. For data analysis, the custom ImageJ plugins
910 used are available at research.stowers.org/imagejplugins/zipped_plugins.html.

911 **Key resources table**

912 See document.

913

914 **Acknowledgments**

915 We thank Claudio Sunkel for antibodies; past and present members of the Hawley lab for
916 helpful discussion and comments on this manuscript especially Satomi Takeo, Cathy Lake,
917 Rachel Nielsen, and Elisabeth Bauerly; Diana Libuda for comments on this manuscript; and
918 Angela Miller for editorial and figure preparation assistance. R.S.H. is an American Cancer
919 Society Research Professor.

920

921 **References**

922 1. Hassold T, Hall H, Hunt P. The origin of human aneuploidy: where we have been, where
923 we are going. Human molecular genetics. 2007;16 Spec No. 2:R203-8. Epub 2007/10/04. doi:
924 10.1093/hmg/ddm243. PubMed PMID: 17911163.

2. Keeney S, Giroux CN, Kleckner N. Meiosis-specific DNA double-strand breaks are catalyzed by Spo11, a member of a widely conserved protein family. Cell. 1997;88(3):375-84. Epub 1997/02/07. PubMed PMID: 9039264.
3. Gray S, Cohen PE. Control of Meiotic Crossovers: From Double-Strand Break Formation to Designation. Annual review of genetics. 2016;50:175-210. doi: 10.1146/annurev-genet-120215-035111. PubMed PMID: 27648641; PubMed Central PMCID: PMCPMC5319444.
4. Hunter N. Meiotic Recombination: The Essence of Heredity. Cold Spring Harb Perspect Biol. 2015. doi: 10.1101/cshperspect.a016618. PubMed PMID: 26511629.
5. Lange J, Yamada S, Tischfield SE, Pan J, Kim S, Zhu X, et al. The Landscape of Mouse Meiotic Double-Strand Break Formation, Processing, and Repair. Cell. 2016;167(3):695-708 e16. doi: 10.1016/j.cell.2016.09.035. PubMed PMID: 27745971; PubMed Central PMCID: PMCPMC5117687.
6. Pan J, Sasaki M, Kniewel R, Murakami H, Blitzblau HG, Tischfield SE, et al. A hierarchical combination of factors shapes the genome-wide topography of yeast meiotic recombination initiation. Cell. 2011;144(5):719-31. doi: 10.1016/j.cell.2011.02.009. PubMed PMID: 21376234; PubMed Central PMCID: PMCPMC3063416.
7. Lake CM, Hawley RS. Becoming a crossover-competent DSB. Semin Cell Dev Biol. 2016;54:117-25. doi: 10.1016/j.semcdb.2016.01.008. PubMed PMID: 26806636.
8. Xiang Y, Miller DE, Ross EJ, Sanchez Alvarado A, Hawley RS. Synaptonemal complex extension from clustered telomeres mediates full-length chromosome pairing in Schmidtea mediterranea. Proc Natl Acad Sci U S A. 2014;111(48):E5159-68. doi: 10.1073/pnas.1420287111. PubMed PMID: 25404302; PubMed Central PMCID: PMCPMC4260563.
9. Miller DE, Smith CB, Kazemi NY, Cockrell AJ, Arvanitakas AV, Blumenstiel JP, et al. Whole-Genome Analysis of Individual Meiotic Events in Drosophila melanogaster Reveals That Noncrossover Gene Conversions Are Insensitive to Interference and the Centromere Effect. Genetics. 2016;203(1):159-71. doi: 10.1534/genetics.115.186486. PubMed PMID: 26944917; PubMed Central PMCID: PMCPMC4858771.
10. Lindsley DL, Sandler L. The genetic analysis of meiosis in female Drosophila melanogaster. Philos Trans R Soc Lond B Biol Sci. 1977;277(955):295-312. PubMed PMID: 16292.
11. Hughes SE, Miller DE, Miller AL, Hawley RS. Female meiosis: synapsis, recombination and segregation in *Drosophila melanogaster*. Genetics. 2017;*in press*.
12. Tanneti NS, Landy K, Joyce EF, McKim KS. A pathway for synapsis initiation during zygotene in Drosophila oocytes. Current biology : CB. 2011;21(21):1852-7. doi: 10.1016/j.cub.2011.10.005. PubMed PMID: 22036181.
13. Christophorou N, Rubin T, Huynh J-R. Synaptonemal Complex Components Promote Centromere Pairing in Pre-Meiotic Germ Cells. PLoS Genet. 2013.
14. Takeo S, Lake CM, Morais-de-Sa E, Sunkel CE, Hawley RS. Synaptonemal complex-dependent centromeric clustering and the initiation of synapsis in Drosophila oocytes. Current biology : CB. 2011;21(21):1845-51. doi: 10.1016/j.cub.2011.09.044. PubMed PMID: 22036182.
15. McKim KS, Green-Marroquin BL, Sekelsky JJ, Chin G, Steinberg C, Khodosh R, et al. Meiotic synapsis in the absence of recombination. Science. 1998;279(5352):876-8. PubMed PMID: 9452390.
16. Mehrotra S, McKim KS. Temporal analysis of meiotic DNA double-strand break formation and repair in Drosophila females. PLoS Genet. 2006;2(11):e200. doi: 10.1371/journal.pgen.0020200. PubMed PMID: 17166055; PubMed Central PMCID: PMCPMC1657055.
17. Libuda DE, Uzawa S, Meyer BJ, Villeneuve AM. Meiotic chromosome structures constrain and respond to designation of crossover sites. Nature. 2013;502(7473):703-6. doi: 10.1038/nature12577. PubMed PMID: 24107990; PubMed Central PMCID: PMCPMC3920622.

18. Hayashi M, Mlynarczyk-Evans S, Villeneuve AM. The synaptonemal complex shapes the crossover landscape through cooperative assembly, crossover promotion and crossover inhibition during Caenorhabditis elegans meiosis. Genetics. 2010;186(1):45-58. doi: 10.1534/genetics.110.115501. PubMed PMID: 20592266; PubMed Central PMCID: PMCPMC2940310.
19. Zickler D, Kleckner N. Recombination, Pairing, and Synapsis of Homologs during Meiosis. Cold Spring Harb Perspect Biol. 2015;7(6). doi: 10.1101/cshperspect.a016626. PubMed PMID: 25986558; PubMed Central PMCID: PMCPMC4448610.
20. Zickler D, Kleckner N. Meiotic chromosomes: integrating structure and function. Annual review of genetics. 1999;33:603-754. doi: 10.1146/annurev.genet.33.1.603. PubMed PMID: 10690419.
21. Cahoon CK, Yu Z, Wang Y, Guo F, Unruh JR, Slaughter BD, et al. Superresolution expansion microscopy reveals the three-dimensional organization of the Drosophila synaptonemal complex. Proc Natl Acad Sci U S A. 2017;114(33):E6857-E66. doi: 10.1073/pnas.1705623114. PubMed PMID: 28760978; PubMed Central PMCID: PMCPMC5565445.
22. Page SL, Hawley RS. c(3)G encodes a Drosophila synaptonemal complex protein. Genes & development. 2001;15(23):3130-43. doi: 10.1101/gad.935001. PubMed PMID: 11731477; PubMed Central PMCID: PMC312841.
23. Anderson LK, Royer SM, Page SL, McKim KS, Lai A, Lilly MA, et al. Juxtaposition of C(2)M and the transverse filament protein C(3)G within the central region of Drosophila synaptonemal complex. Proc Natl Acad Sci U S A. 2005;102(12):4482-7. doi: 10.1073/pnas.0500172102. PubMed PMID: 15767569; PubMed Central PMCID: PMC555515.
24. Collins KA, Unruh JR, Slaughter BD, Yu Z, Lake CM, Nielsen RJ, et al. Corolla Is a Novel Protein that Contributes to the Architecture of the Synaptonemal Complex of Drosophila. Genetics. 2014. doi: 10.1534/genetics.114.165290. PubMed PMID: 24913682.
25. Page SL, Khetani RS, Lake CM, Nielsen RJ, Jeffress JK, Warren WD, et al. Corona is required for higher-order assembly of transverse filaments into full-length synaptonemal complex in Drosophila oocytes. PLoS Genet. 2008;4(9):e1000194. doi: 10.1371/journal.pgen.1000194. PubMed PMID: 18802461; PubMed Central PMCID: PMC2529403.
26. Lake CM, Hawley RS. The molecular control of meiotic chromosomal behavior: events in early meiotic prophase in Drosophila oocytes. Annu Rev Physiol. 2012;74:425-51. doi: 10.1146/annurev-physiol-020911-153342. PubMed PMID: 22335798.
27. Jeffress JK, Page SL, Royer SK, Belden ED, Blumenstiel JP, Anderson LK, et al. The formation of the central element of the synaptonemal complex may occur by multiple mechanisms: the roles of the N- and C-terminal domains of the Drosophila C(3)G protein in mediating synapsis and recombination. Genetics. 2007;177(4):2445-56. doi: 10.1534/genetics.107.078717. PubMed PMID: 17947423; PubMed Central PMCID: PMC2219479.
28. Tung KS, Roeder GS. Meiotic chromosome morphology and behavior in zip1 mutants of Saccharomyces cerevisiae. Genetics. 1998;149(2):817-32. PubMed PMID: 9611194; PubMed Central PMCID: PMC1460213.
29. Lake CM, Nielsen RJ, Guo F, Unruh JR, Slaughter BD, Hawley RS. Vilya, a component of the recombination nodule, is required for meiotic double-strand break formation in Drosophila. eLife. 2015;4:e08287. doi: 10.7554/eLife.08287. PubMed PMID: 26452093; PubMed Central PMCID: PMCPMC4703084.
30. Lake CM, Holsclaw JK, Bellendir SP, Sekelsky J, Hawley RS. The development of a monoclonal antibody recognizing the Drosophila melanogaster phosphorylated histone H2A variant (gamma-H2AV). G3 (Bethesda). 2013;3(9):1539-43. doi: 10.1534/g3.113.006833. PubMed PMID: 23833215; PubMed Central PMCID: PMCPMC3755914.

1027 31. Zickler D, Kleckner N. A few of our favorite things: Pairing, the bouquet, crossover
1028 interference and evolution of meiosis. Semin Cell Dev Biol. 2016;54:135-48. doi:
1029 10.1016/j.semcdb.2016.02.024. PubMed PMID: 26927691; PubMed Central PMCID:
1030 PMCPMC4867269.
1031 32. Gowen JW. Meiosis as a genetic character in *Drosophila melanogaster*. The Journal of
1032 Experiment Zoology. 1933;65(1):83-106.
1033 33. Hall JC. Chromosome segregation influenced by two alleles of the meiotic mutant c(3)G
1034 in Drosophila melanogaster. Genetics. 1972;71(3):367-400. PubMed PMID: 4624918.
1035 34. Miller DE. Genomic analysis of meiosis in *Drosophila melanogaster* [dissertation].
1036 Kansas City, KS: University of Kansas Medical Center; 2016.
1037 35. Ashburner M, Golic KG, Hawley RS. Drosophila: A laboratory handbook. 2 ed. Cold
1038 Spring Harbor, New York: Cold Spring Harbor Laboratory Press; 2005.
1039 36. Weinstein A. Coincidence of Crossing over in DROSOPHILA MELANOGASTER
1040 (AMPELOPHILA). Genetics. 1918;3(2):135-72. PubMed PMID: 17245901; PubMed Central
1041 PMCID: PMCPMC1200433.
1042 37. Yan R, McKee BD. The cohesion protein SOLO associates with SMC1 and is required
1043 for synapsis, recombination, homolog bias and cohesion and pairing of centromeres in
1044 Drosophila Meiosis. PLoS Genet. 2013;9(7):e1003637. doi: 10.1371/journal.pgen.1003637.
1045 PubMed PMID: 23874232; PubMed Central PMCID: PMC3715423.
1046 38. Mason JM. Orientation disruptor (ord): a recombination-defective and disjunction-
1047 defective meiotic mutant in Drosophila melanogaster. Genetics. 1976;84(3):545-72. PubMed
1048 PMID: 826453; PubMed Central PMCID: PMCPMC1213594.
1049 39. Baker BS, Hall JC. Meiotic mutants: genie control of meiotic recombination and
1050 chromosome segregation. In: Ashburner M, Novitski E, editors. The Genetics and Biology of
1051 Drosophila. 1a. New York: Academic Press; 1976.
1052 40. Hawley RS, Irick H, Zitron AE, Haddox DA, Lohe A, New C, et al. There are two
1053 mechanisms of achiasmate segregation in Drosophila females, one of which requires
1054 heterochromatic homology. Dev Genet. 1992;13(6):440-67. doi: 10.1002/dvg.1020130608.
1055 PubMed PMID: 1304424.
1056 41. Hawley RS, Theurkauf WE. Requiem for distributive segregation: achiasmate
1057 segregation in Drosophila females. Trends Genet. 1993;9(9):310-7. PubMed PMID: 8236460.
1058 42. Balicky EM, Endres MW, Lai C, Bickel SE. Meiotic cohesion requires accumulation of
1059 ORD on chromosomes before condensation. Molecular biology of the cell. 2002;13(11):3890-
1060 900. doi: 10.1091/mbc.E02-06-0332. PubMed PMID: 12429833; PubMed Central PMCID:
1061 PMC133601.
1062 43. Khetani RS, Bickel SE. Regulation of meiotic cohesion and chromosome core
1063 morphogenesis during pachytene in Drosophila oocytes. Journal of cell science. 2007;120(Pt
1064 17):3123-37. doi: 10.1242/jcs.009977. PubMed PMID: 17698920.
1065 44. Krishnan B, Thomas SE, Yan R, Yamada H, Zhulin IB, McKee BD. Sisters unbound is
1066 required for meiotic centromeric cohesion in Drosophila melanogaster. Genetics.
1067 2014;198(3):947-65. doi: 10.1534/genetics.114.166009. PubMed PMID: 25194162; PubMed
1068 Central PMCID: PMCPMC4224182.
1069 45. Yan R, Thomas SE, Tsai JH, Yamada Y, McKee BD. SOLO: a meiotic protein required
1070 for centromere cohesion, coorientation, and SMC1 localization in Drosophila melanogaster. The
1071 Journal of cell biology. 2010;188(3):335-49. doi: 10.1083/jcb.200904040. PubMed PMID:
1072 20142422; PubMed Central PMCID: PMC2819681.
1073 46. Gladstone MN, Obeso D, Chuong H, Dawson DS. The synaptonemal complex protein
1074 Zip1 promotes bi-orientation of centromeres at meiosis I. PLoS Genet. 2009;5(12):e1000771.
1075 doi: 10.1371/journal.pgen.1000771. PubMed PMID: 20011112; PubMed Central PMCID:
1076 PMC2781170.

1077 47. Kurdzo EL, Obeso D, Chuong H, Dawson DS. Meiotic Centromere Coupling and Pairing
1078 Function by Two Separate Mechanisms in Saccharomyces cerevisiae. Genetics.
1079 2017;205(2):657-71. doi: 10.1534/genetics.116.190264. PubMed PMID: 27913618; PubMed
1080 Central PMCID: PMCPMC5289843.
1081 48. Qiao H, Chen JK, Reynolds A, Hoog C, Paddy M, Hunter N. Interplay between
1082 synaptonemal complex, homologous recombination, and centromeres during mammalian
1083 meiosis. PLoS Genet. 2012;8(6):e1002790. doi: 10.1371/journal.pgen.1002790. PubMed PMID:
1084 22761591; PubMed Central PMCID: PMC3386176.
1085 49. Carpenter A. Thoughts on recombination nodules, meiotic recombination, and
1086 chiasmata. In: Kucherlapati R, Smith GR, editors. Genetic Recombination. Washington, DC:
1087 American Society for Microbiology; 1988. p. 529-48.
1088 50. Mlynarczyk-Evans S, Villeneuve AM. Time-Course Analysis of Early Meiotic Prophase
1089 Events Informs Mechanisms of Homolog Pairing and Synapsis in Caenorhabditis elegans.
1090 Genetics. 2017;207(1):103-14. doi: 10.1534/genetics.117.204172. PubMed PMID: 28710064;
1091 PubMed Central PMCID: PMCPMC5586365.
1092 51. Jaramillo-Lambert A, Ellefson M, Villeneuve AM, Engebrecht J. Differential timing of S
1093 phases, X chromosome replication, and meiotic prophase in the C. elegans germ line. Dev Biol.
1094 2007;308(1):206-21. doi: 10.1016/j.ydbio.2007.05.019. PubMed PMID: 17599823.
1095 52. Olivier N, Keller D, Rajan VS, Gonczy P, Manley S. Simple buffers for 3D STORM
1096 microscopy. Biomed Opt Express. 2013;4(6):885-99. doi: 10.1364/BOE.4.000885. PubMed
1097 PMID: 23761850; PubMed Central PMCID: PMCPMC3675867.
1098 53. Harris D, Orme C, Kramer J, Namba L, Champion M, Palladino MJ, et al. A deficiency
1099 screen of the major autosomes identifies a gene (matrimony) that is haplo-insufficient for
1100 achiasmate segregation in Drosophila oocytes. Genetics. 2003;165(2):637-52. PubMed PMID:
1101 14573476; PubMed Central PMCID: PMCPMC1462769.
1102 54. Matthies HJG, Clarkson M, Saint RB, Namba R, Hawley RS. Analysis of meiosis in fixed
1103 and live oocytes by light microscopy. In: Sullivan W, Ashburner M, Hawley RS, editors.
1104 *Drosophila* protocols. Cold Spring Harbor, New York: Cold Spring Harbor Laboratory Press;
1105 2000. p. 67-86.
1106 55. Ovesny M, Krizek P, Borkovec J, Svindrych Z, Hagen GM. ThunderSTORM: a
1107 comprehensive ImageJ plug-in for PALM and STORM data analysis and super-resolution
1108 imaging. Bioinformatics. 2014;30(16):2389-90. doi: 10.1093/bioinformatics/btu202. PubMed
1109 PMID: 24771516; PubMed Central PMCID: PMCPMC4207427.
1110 56. Burns S, Avena JS, Unruh JR, Yu Z, Smith SE, Slaughter BD, et al. Structured
1111 illumination with particle averaging reveals novel roles for yeast centrosome components during
1112 duplication. eLife. 2015;4. doi: 10.7554/eLife.08586. PubMed PMID: 26371506; PubMed Central
1113 PMCID: PMCPMC4564689.
1114 57. Hawley RS, Walker MY. Advanced Genetic Analysis. Malden, MA: Blackwell Publishing;
1115 2009.

1116

1117

1118

1119

Figure Legends

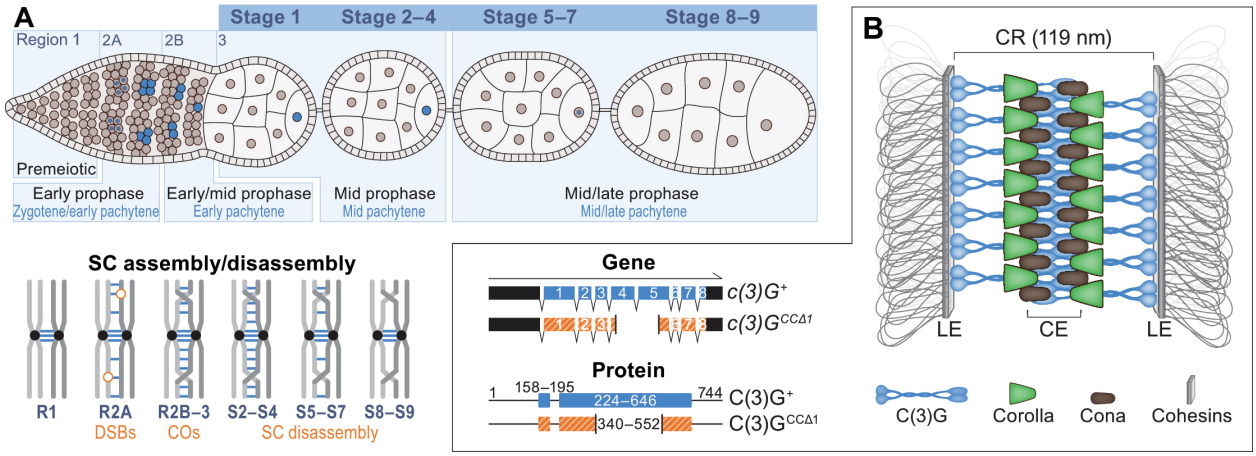

Figure 1: Background on Drosophila female meiosis and the SC

(A) Diagram of Drosophila female meiosis, which is described in [11]. Briefly, at the anterior tip of the germarium is a germline stem cell that divides asymmetrically to give rise to a cystoblast, which undergoes four mitotic divisions with incomplete cytokinesis to give rise to a 16-cell cyst. Homologous chromosome pairing and SC assembly begin at the centromeres (represented as black dots on the chromosomes) during these mitotic divisions [13]. Then, four cells in the 16-cell cyst officially enter meiosis in region 2A (zygotene/early pachytene) by assembling the SC along the chromosome arms. During region 2A, DNA double-strand breaks (DSBs) are formed within the context of the SC, starting meiotic recombination. By region 2B (early pachytene), the fully synapsed cells have started to repair their DSBs and two of the four cells have backed out of the meiotic program. By region 3 (mid pachytene), the oocyte nucleus has been selected and is the only nucleus within the cyst that retains the SC—all other nuclei have backed out of meiosis and have disassembled their SC to become nurse cells. Additionally, all the DSBs are in the processes of being repaired into crossovers (COs) or noncrossovers by region 3. After the germarium, the oocyte continues to develop and the SC is maintained along the chromosome arms until stage 5. From stages 5–7 (mid/late pachytene), the SC is disassembled from multiple regions along the chromosome arms, but the SC persists at the centromere into

1139 the later stages of prophase I (stages8–9) [12, 14]. (B) Model of the Drosophila SC with the
1140 transverse filament protein C(3)G in blue, the central region (CR) protein Corolla in green, the
1141 central element protein (CE) CONA in brown, and the lateral element (LE)/cohesin proteins
1142 represented by gray (adapted from [11]). Next to the SC model are diagrams of the gene and
1143 protein structures for wild type C(3)G^{+} (blue) and *c(3)G*^{ccΔ1} (orange).

1144

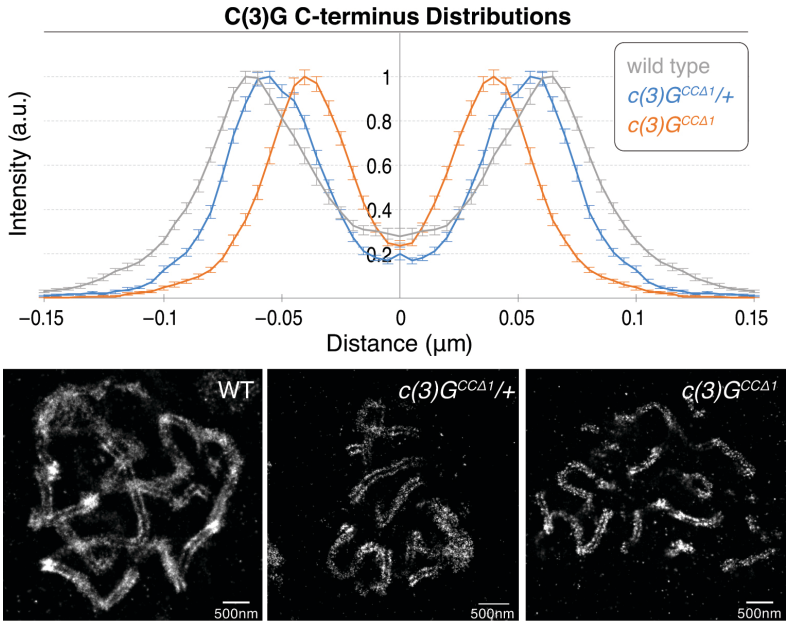

1145

1146 **Figure 2: STORM analysis of the SC structure in *c(3)G*^{ccΔ1} mutants**

1147 STORM images of intact germaria with the C-terminus of C(3)G labeled in wild type (WT, grey),
1148 *c(3)G*^{ccΔ1} heterozygotes (*c(3)G*^{ccΔ1}*/+,* blue) and homozygotes (*c(3)G*^{ccΔ1}, orange). The
1149 quantification above the images displays the average distribution of the two C-terminal C(3)G
1150 tracks based on the line profile analysis of each genotype (see Methods). The quantification
1151 resulted an average width of 119nm ± SE 1.0nm in WT, 107nm ± SE 0.4nm in *c(3)G*^{ccΔ1}
1152 heterozygotes, and 78.6nm ± SE 0.3nm in *c(3)G*^{ccΔ1} homozygotes. The average distribution was
1153 generated by averaging 26 line profiles from 8 WT nuclei, 34 line profiles from 17 *c(3)G*^{ccΔ1}
1154 heterozygous nuclei, and 32 line profiles from 13 *c(3)G*^{ccΔ1} heterozygous nuclei.

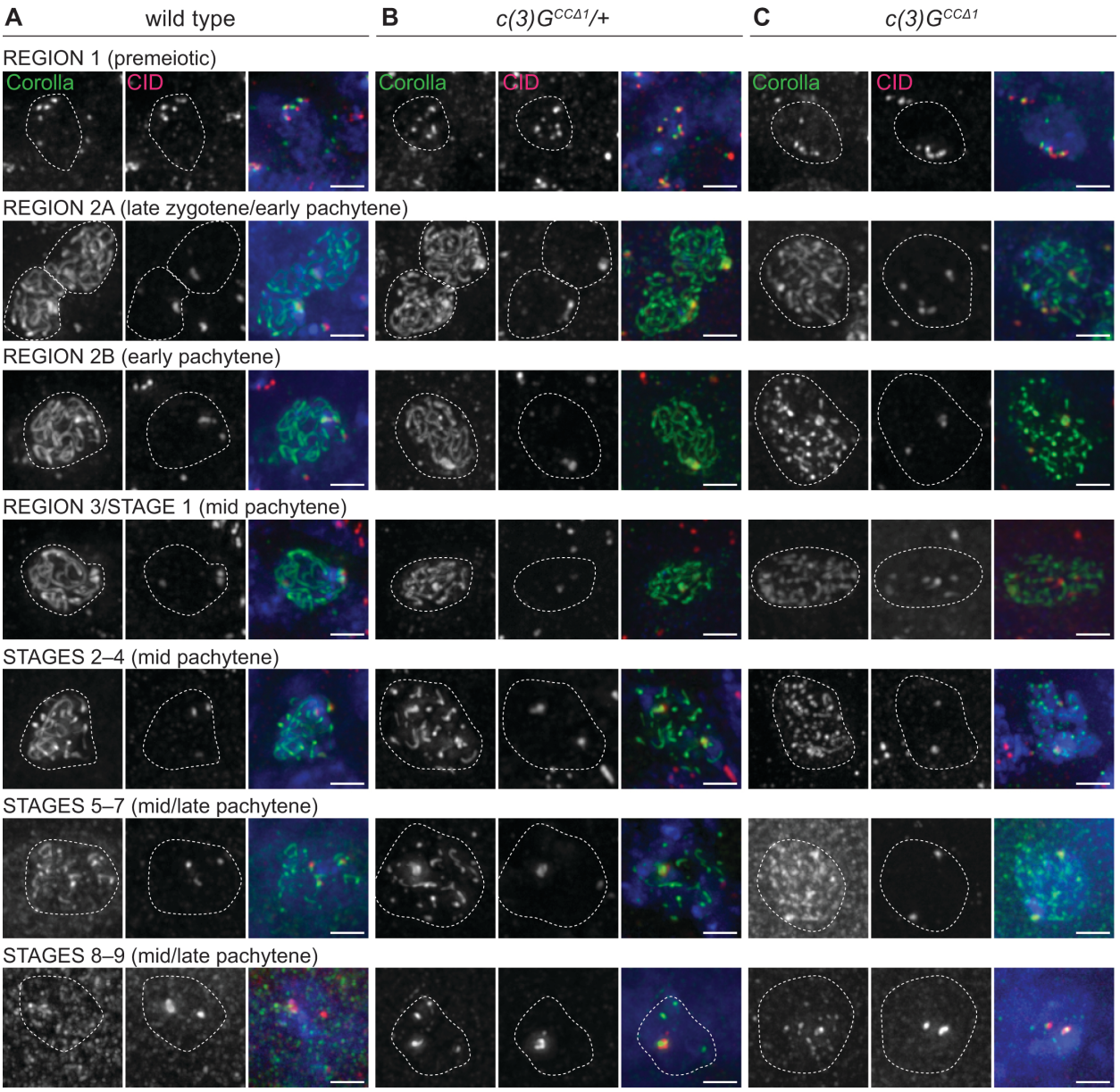

Figure 3: Euchromatic SC prematurely disassembles in both *c(3)G^{ccΔ1}* homozygotes and heterozygotes

(A) Images showing localization of the SC protein Corolla (green), the centromeric nucleosome CID (red) and DAPI-stained DNA (blue) in wild type (A), *c(3)G^{ccΔ1}*/+ heterozygotes (B), and *c(3)G^{ccΔ1}* homozygotes (C) from zygotene/early pachytene (region 2A) to mid/late pachytene (stages 8–9). Dotted lines indicate the location of the nucleus as defined by DAPI staining (blue). Scale bars, 2 μm.

1163

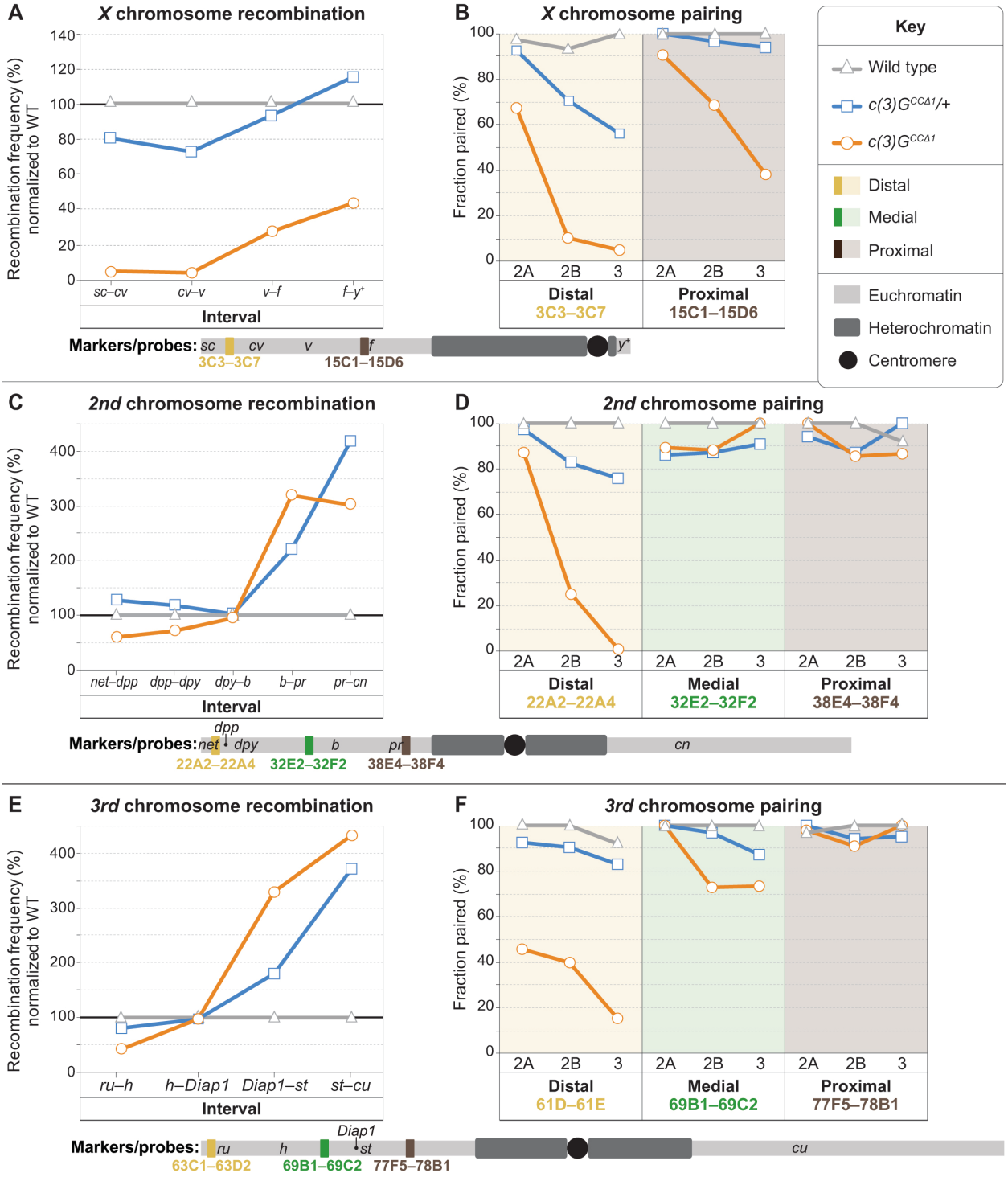

1164

1165 **Figure 4: *c(3)G*^{ccΔ1} causes changes in recombination and euchromatic pairing on the *X*,**
1166 ***2*nd and *3*rd chromosomes**

1167 The frequency of recombination (A, C, E) and the fraction of euchromatic pairing (B, D, F) in
1168 wild type (WT, grey triangles), *c(3)G*^{ccΔ1} heterozygotes [*c(3)G*^{ccΔ1}/+, blue squares] and
1169 homozygotes [*c(3)G*^{ccΔ1}, orange circles] at distal (yellow), medial (green) and proximal (brown)
1170 loci on the *X*, *2*nd and *3*rd chromosomes. The markers used to assay recombination on the *X*
1171 chromosome are *scute* (*sc*), *crossveinless* (*cv*), *vermillion* (*v*), *forked* (*f*), and *yellow*$^{+}$ (*y*$^{+}$,
1172 integrated wild type allele). (The multiply marked *X* chromosome also carries a null mutant of
1173 the *yellow* gene at the genomic locus, see Methods.) The markers used to assay recombination
1174 on the *2*nd chromosome are *net, decapentaplegic* (*dpp*), *dumpy* (*dpy*), *black* (*b*), *purple* (*pr*), and
1175 *cinnabar* (*cn*). The markers used to assay recombination on the *3*rd chromosome are *roughoid*
1176 (*ru*), *hairy* (*h*), *thread* (*th*), *scarlet* (*st*), and *curled* (*cu*). For reference, below each set of charts is
1177 a diagram of the corresponding chromosome being analyzed displaying the relative positions of
1178 the recombination markers, locations of each FISH probe and the approximate amounts of
1179 pericentromeric heterochromatin estimated from [35] (the black circle represents the
1180 centromere; the chromosome diagrams do not include telomeric heterochromatin). The genomic
1181 positions of all the markers and pairing probes within the figure are in Table S2 (base pair
1182 numbers from flybase release FB2017_06).

1183

1184

1185

1186

1187

1188

1189

1190

1191 **Supplemental Figure Legends**

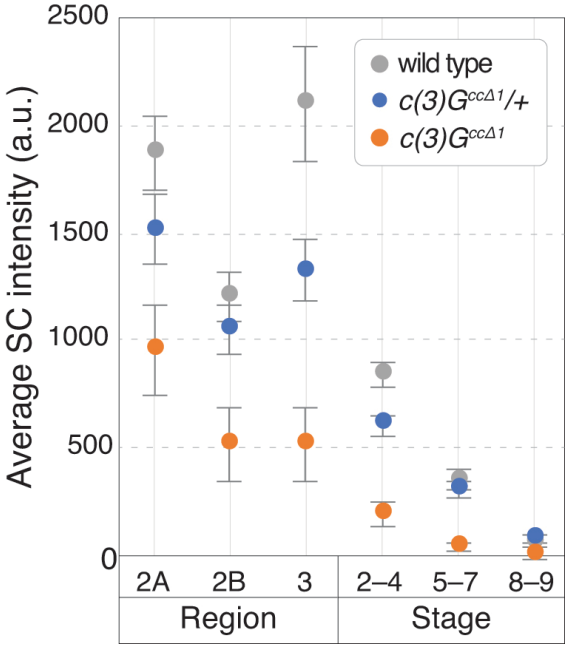

1192

1193 **Figure S1: SC intensity quantification**

1194 Average intensity of the Corolla antibody staining for wild type (grey), *c(3)G*^{ccΔ1} heterozygotes
1195 (*ccΔ1/+*, blue) and homozygotes (*ccΔ1*, orange) from zygotene/early pachytene (region 2A) to
1196 mid/late pachytene (stage 8–9). (See Methods for the detailed description of how this analysis
1197 was performed). For WT, the average intensity was generated by averaging measurements
1198 from 19 nuclei in region 2A, 18 nuclei in region 2B, 12 nuclei in region 3, 49 nuclei from stages
1199 2–4, 39 nuclei from stages 5–7, and 18 nuclei from stages 8–9. For *c(3)G*^{ccΔ1} heterozygotes, the
1200 average intensity was generated by averaging measurements from 16 nuclei in region 2A, 13
1201 nuclei in region 2B, 19 nuclei in region 3, 46 nuclei from stages 2–4, 47 nuclei from stages 5–7,
1202 and 34 nuclei from stages 8–9. For *c(3)G*^{ccΔ1} homozygotes, the average intensity was generated
1203 by averaging measurements from 18 nuclei in region 2A, 11 nuclei in region 2B,16 nuclei in
1204 region 3, 42 nuclei from stages 2–4, 47 nuclei from stages 5–7, and 31 nuclei from stages 8–9.

1205

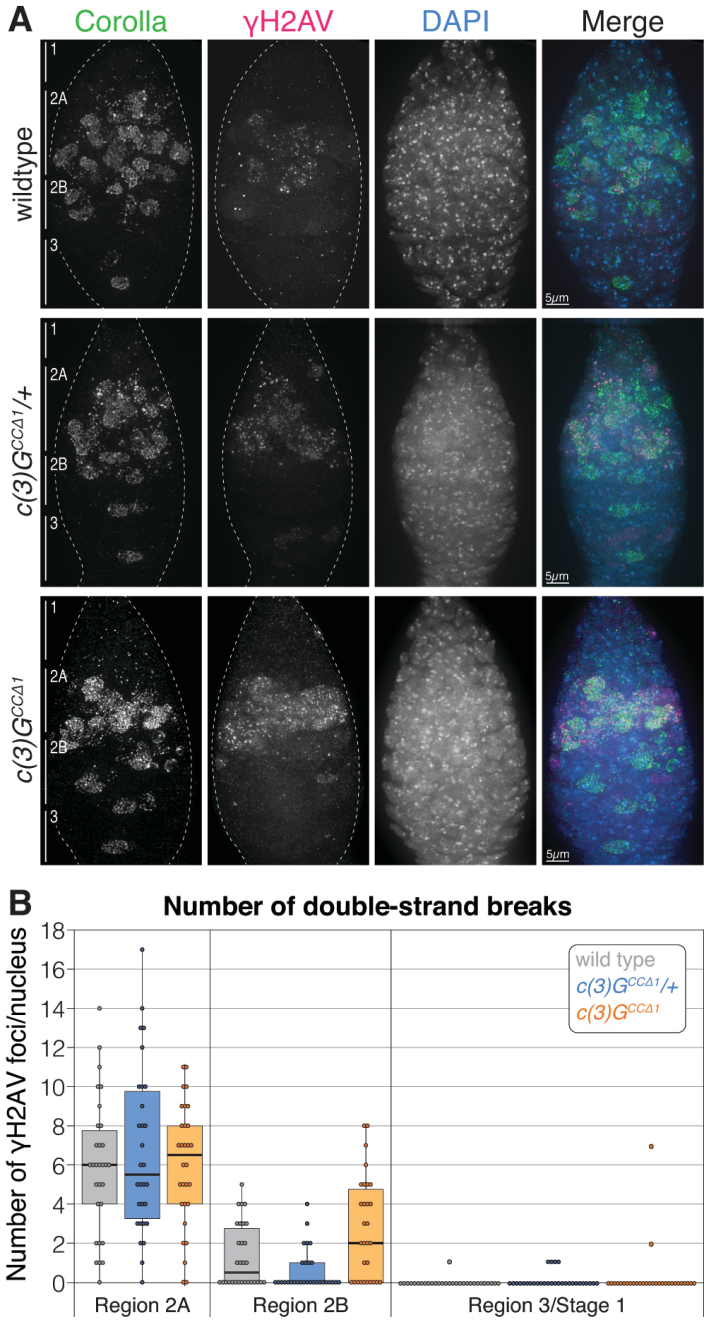

1206

1207 **Figure S2: The formation of double-strand breaks is normal in *c(3)G^{ccΔ1}* mutants**

1208 (A) Images of the germarium stained with the SC protein Corolla (green), γH2AV (magenta) and

1209 DAPI (blue) in WT and *c(3)G^{ccΔ1}* heterozygotes (*c(3)G^{ccΔ1}*/+) and homozygotes (*c(3)G^{ccΔ1}*).

1210 Region 1, 2A, 2B, and 3 are labeled on the images as a reference. (B) Quantification of the

1211 number of DNA double-strand breaks as assayed by counting the number of γH2AV foci per

1212 nucleus in each region of the germarium for WT and *c(3)G*^{ccΔ1} heterozygotes (*c(3)G*^{ccΔ1}/+) and

1213 homozygotes (*c(3)G*^{ccΔ1}).

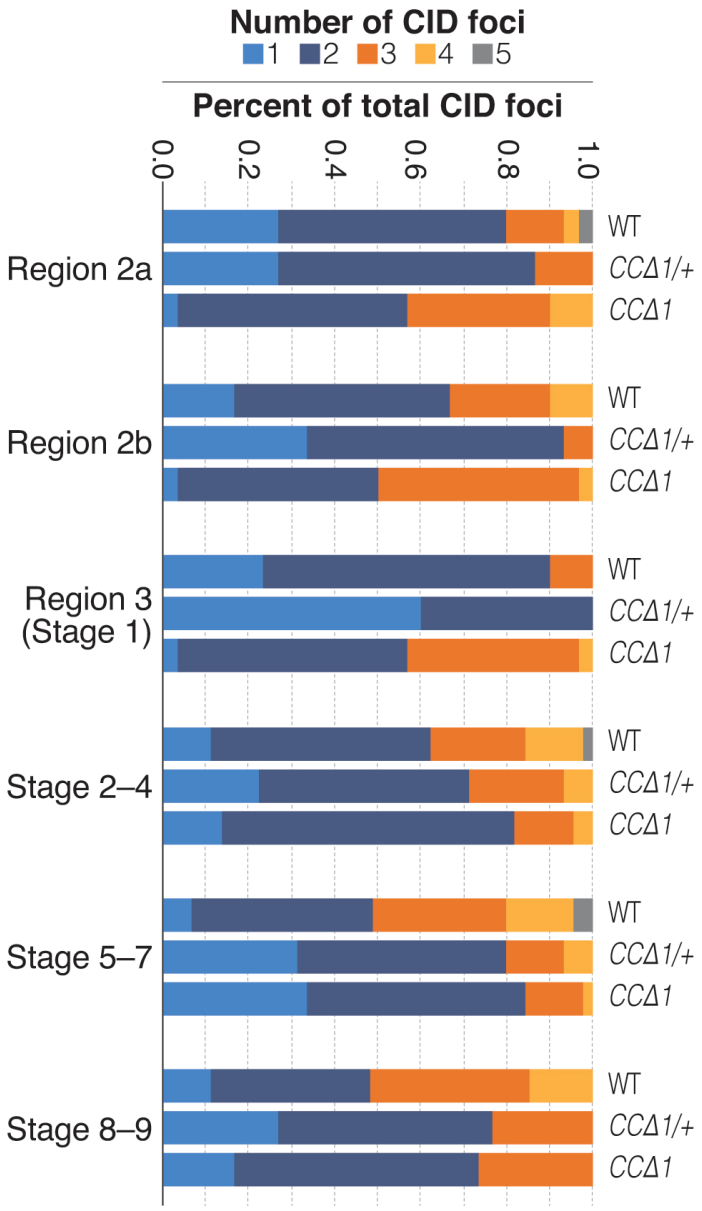

1214

1215 **Figure S3: Centromeric SC is unaffected by the *c(3)G*^{ccΔ1} mutation**

1216 Quantification of the percent of CID foci per nucleus in WT, *c(3)G*^{ccΔ1} heterozygotes (*ccΔ1/+*),

1217 and homozygotes (*ccΔ1*) from zygotene/early pachytene (region 2A) to mid/late pachytene

1218 (stage 8–9). (See Methods for a description of how this quantification was performed.)

1219 **Tables**

Table 1. *X* Chromosome Recombination			
Maternal genotype	*yw; pol*	*c(3)G*^{ccΔ1}/+	*c(3)G*^{ccΔ1}
	(N = 1515)	(N = 1289)	(N = 1420)
Map Length			
sc–cv	8.8	7.1	0.4
cv–v	20.7	11.9	0.7
v–f	21.1	17.7	5.2
f–y^{+}	12.4	14.4	5.4
Total	**63.0**	**51.2**	**11.8**
Interference			
sc/cv/v	0.7	0.9	1.0
cv/v/f	0.6	0.9	1.0
v/f/y^{+}	0.7	0.9	0.9
Class			
NCO	688	702	1264
SCO	703	512	147
DCO	120	67	7
TCO	4	3	2
Exchange rank			
E_0	0.067	0.201	0.790
E_1	0.627	0.600	0.196
E_2	0.285	0.180	0.003
E_3	0.021	0.019	0.011
E_4	0	0	0

1220 Abbreviations: N, total number of flies scored; NCO, chromatids recovered exhibiting no
1221 crossovers; SCO, single-crossover chromatids; DCO, double-crossover chromatids; TCO, triple-
1222 crossover chromatids.

1223

1224

1225

1226

1227

1228

1229

Table 2. *2nd* Chromosome Recombination			
Maternal genotype	*yw; pol*	*c(3)G^{ccΔ1}/+*	*c(3)G^{ccΔ1}*
	(N = 2376)	(N = 2471)	(N = 1456)
Map Length			
net–dpp	5.7	7.2	3.4
dpp–dpy	8.0	9.5	5.8
dpy–b	28.5	29.5	26.9
b–pr	7.8	17.2	24.9
pr–cn	2.2	9.3	6.7
Total	**52.2**	**72.8**	**67.6**
Interference			
net/dpp/dpy	0.3	–0.7	0.8
dpp/dpy/b	0.6	–0.2	0.8
dpy/b/pr	0.6	–0.2	–0.2
b/pr/cn	–0.2	–5.3	–2.2
Class			
NCO	1249	1001	624
SCO	1021	1180	692
DCO	98	255	128
TCO	8	35	12
QCO	0	1	0
Exchange rank			
E_0	0.134	0.017	0.033
E_1	0.715	0.624	0.648
E_2	0.125	0.253	0.253
E_3	0.027	0.100	0.066
E_4	0	0.006	0

1230 Abbreviations: N, total number of flies scored; NCO, chromatids recovered exhibiting no
1231 crossovers; SCO, single-crossover chromatids; DCO, double-crossover chromatids; TCO, triple-
1232 crossover chromatids; QCO, quadruple-crossover chromatid.

1233

1234

1235

1236

1237

1238

1239

Table 3. *3rd* Chromosome Recombination			
Maternal genotype	*yw; pol*	*c(3)G^{ccΔ1}/+*	*c(3)G^{ccΔ1}*
	(N = 1014)	(N = 1027)	(N = 1485)
Map Length			
ru–hu	22.4	18.4	9.5
h–th	21.8	21.5	21.7
th–st	0.6	1.1	2.0
st–cu	6.1	22.8	26.5
Total	**50.9**	**63.8**	**59.6**
Interference			
ru/h/th	0.7	0.9	0.5
h/th/st	1	1	0.2
th/st/cu	–4.5	–4.5	–12.6
Class			
NCO	574	465	746
SCO	420	470	586
DCO	45	91	146
TCO	2	1	6
Exchange rank			
E_0	0.168	0.083	0.202
E_1	0.663	0.567	0.420
E_2	0.154	0.343	0.345
E_3	0.016	0.008	0.032
E_4	0	0	0

1240 Abbreviations: N, total number of flies scored; NCO, chromatids recovered exhibiting no
1241 crossovers; SCO, single-crossover chromatids; DCO, double-crossover chromatids; TCO, triple-
1242 crossover chromatids.

1243

1244

1245

1246

1247

1248

1249

1250

Table S1: Average number of CID foci per stage of oogenesis*

	Stage 1					
	Region 2a	**Region 2b**	**Region 3**	**Stage 2-4**	**Stage 5-7**	**Stage 8-9**
WT	2.0±SD 0.9 (30)	2.3±SD 0.9 (30)	1.9±SD 0.6 (30)	2.4±SD 0.9 (45)	2.7±SD 1.0 (45)	2.6±SD 0.9 (27)
c(3)G^{ccΔ1}/+	1.9±SD 0.6 (30)	1.7±SD 0.6 (30)	1.4±SD 0.5 (30)	2.4±SD 0.8 (45)	2.0± SD 0.9 (45)	2.0±SD 0.7 (30)
c(3)G^{ccΔ1}	2.5±SD 0.7 (30)	2.5±SD 0.6 (30)	2.4±SD 0.6 (30)	2.1±SD 0.7 (44)	1.8± SD 0.7 (45)	2.1±SD 0.7 (30)

* SD=standard deviation; (n)=number of nuclei score

Table S2: Genomic locations of recombination markers and pairing probes (from flybase release FB2017_06)

	Symbol/Band*	Genomic location**
X chromosome recombination markers	*sc*	*XL*: 396,060
	cv	*XL*: 5,690,002
	v	*XL*: 10,923,972
	f	*XL*: 17,232,942
	y+	*XR*: unknown
2nd chromosome recombination markers	*net*	*2L*: 82,421
	dpp	*2L*: 2,428,372
	dpy	*2L*: 4,477,462
	b	*2L*: 13,821,248
	pr	*2L*: 20,073,719
	cn	2R: 7,782,797
3rd chromosome recombination markers	*ru*	*3L*: 1,370,628
	h	*3L*: 8,675,759
	Diap1	*3L*: 16,038,410
	st	*3L*: 16,497,651
	cu	*3R*: 11,197,592
X chromosome pairing probes	3C3–3C7	*XL*: 2,907,702–3,141,427
	15C1–15D6	*XL*: 16,900,783–17,066,397
2nd chromosome pairing probes	22A2–22A4	*2L*: 1,428,615–1,645,199
	32E2–32F2	*2L*: 11,217,687–11,538,470
	38E4–38F4	*2L*: 20,722,927–20,910,490
3rd chromosome pairing probes	63C1–63D2	*3L*: 756,009–1,080,330
	69B1–69C2	*3L*: 12,298,256–12,491,589
	77F5–78B1	*3L*: 20,914,572–21,101,191

*Symbol = gene symbol of marker allele used to score recombination; band = location along polytene chromosome of probe used to score pairing
**Molecular location of each marker/probe is approximate

Table S3: Percent paired at each euchromatic locus assayed*

Chromosome *2L*

	Distal (2809:22A2-22A4)			Medial (43K24:32E2-32F2)			Proximal (7D17:38E4-38F4)		
Genotype	**2a**	**2b**	**3**	**2a**	**2b**	**3**	**2a**	**2b**	**3**
WT	100% (21)	100% (20)	100% (13)	100% (21)	100% (15)	100% (8)	100% (25)	100% (23)	92.3% (13)
$c(3)G^{cc\Delta1}$/+	97.7% (44)	82.6% (23)	76.2% (21)	86.2% (29)	87.5% (24)	90.9% (11)	94.1% (34)	87.1% (31)	100% (16)
$c(3)G^{cc\Delta1}$	87.5% (24)	25% (20)	1% (9)	89.7% (29)	88.2% (17)	100% (7)	100% (37)	85.7% (28)	86.7% (15)

Chromosome *3L*

	Distal (2N23:61D-61E)			Medial (26C20:69B1-69C2)			Proximal (3J2:77F5-78B1)		
Genotype	**2a**	**2b**	**3**	**2a**	**2b**	**3**	**2a**	**2b**	**3**
WT	100% (25)	100% (23)	92.3% (13)	100% (31)	100% (25)	100% (13)	97.1% (35)	100% (34)	100% (14)
$c(3)G^{cc\Delta1}$/+	92.6% (27)	90.3% (21)	83.3% (18)	100% (32)	96.8% (31)	87.5% (16)	100% (36)	94.4% (36)	95.5% (22)
$c(3)G^{cc\Delta1}$	45.8% (24)	40% (20)	15.4% (13)	100% (33)	73.1% (26)	73.68% (19)	98.1% (54)	90.9% (33)	100% (17)

Chromosome *X*

	Distal (3D13:3C3-3C7)			Proximal (9H1:15C1-15D6)		
Genotype	**2a**	**2b**	**3**	**2a**	**2b**	**3**
WT	97.4% (38)	93.8% (32)	100% (13)	100% (43)	100% (44)	100% (18)
$c(3)G^{cc\Delta1}$/+	92.9% (42)	71.0% (31)	56.3% (16)	100% (35)	97.1% (35)	94.1% (17)
$c(3)G^{cc\Delta1}$	67.9% (28)	10.7% (28)	5.3% (19)	90.6% (32)	69.0% (29)	38.5% (13)

*(n) = number of nuclei scored

Table S4: Nondisjuction of *X* and *4*th chromosomes

	Maternal genotype		
	yw; pol	*c(3)G*^{ccΔ1}/+	*c(3)G*^{ccΔ1}
Adj. total	1348	1655	954
% X	0.7	0.2	1.5
% 4	0.4	0.1	0.6